Representing the Dynamic Response of Vegetation to Nitrogen Limitation in the CLASSIC Land Model

Sian Kou-Giesbrecht[1]* and Vivek K. Arora[1]

[1]Canadian Centre for Climate Modelling and Analysis, Environment and Climate Change Canada, Victoria, B.C., Canada.

Corresponding author: Sian Kou-Giesbrecht (sian.kougiesbrecht@ec.gc.ca)

Key Points:

- The dynamic response of vegetation to nitrogen limitation is critical for projecting the terrestrial carbon sink with land models
- Upregulated biological nitrogen fixation driven by stronger nitrogen limitation under elevated CO_2 alleviates nitrogen limitation
- This determines the response of terrestrial carbon and nitrogen cycling to CO_2, nitrogen deposition, and other global change drivers

Abstract

Despite its pivotal feedback to carbon cycling, representing the dynamic response of vegetation to nitrogen limitation is a key challenge for simulating the terrestrial carbon sink in land models. Here, we explore a representation of this dynamic response of vegetation to nitrogen limitation with a novel representation of biological nitrogen fixation and nitrogen cycling in the Canadian Land Surface Scheme Including Biogeochemical Cycles (CLASSIC) model. First, we assess how incorporating this dynamic response of vegetation to nitrogen limitation via biological nitrogen fixation influences carbon sequestration for CO_2 and nitrogen fertilisation experiments, comparing simulations against observation-based estimates from meta-analyses. This evaluates whether underlying mechanisms are realistically represented. Second, we assess how incorporating the dynamic response of vegetation to nitrogen limitation via biological nitrogen fixation affects carbon sequestration over the late 20th and early 21st century, examining the effects of global change drivers (CO_2, nitrogen deposition, climate, and land use change) acting both individually and concurrently. Including nitrogen cycling reduces the terrestrial carbon sink driven by elevated atmospheric CO_2 concentration over the historical period. Representing the dynamic response of vegetation to nitrogen limitation via biological nitrogen fixation increases the present-day terrestrial carbon sink by 0.2 Pg C yr^{-1} because the upregulation of biological nitrogen fixation driven by stronger nitrogen limitation under elevated atmospheric CO_2 concentration alleviates nitrogen limitation. Our results highlight the importance of the dynamic response of vegetation to nitrogen limitation for realistically projecting the future terrestrial carbon sink under global change with land models.

1 Introduction

Terrestrial ecosystems sequester approximately a quarter of anthropogenic CO_2 emissions (Friedlingstein et al., 2019; Le Quéré et al., 2018). However, the persistence of the terrestrial carbon (C) sink is dependent on the availability of nitrogen (N), which is an essential limiting nutrient to plant growth across terrestrial ecosystems (Elser et al., 2007; LeBauer & Treseder, 2008; Wright et al., 2018). Land models are widely applied within the framework of Earth System Models to simulate the terrestrial C sink and inform climate change mitigation policy (Arora et al., 2020). Coupled C and N cycling is a recent progression in land models and there are a multitude of uncertainties in its representation due to the complexity of terrestrial N cycle processes (Davies-Barnard et al., 2020). As a result, the influence of N limitation of plant growth on the terrestrial C sink remains uncertain in land models (Thomas et al., 2015).

A key challenge is representing the capacity of vegetation to dynamically respond to N limitation. In particular, the representation of biological N fixation (BNF), which is the conversion of atmospheric nitrogen gas (N_2) to a plant-available form of N by bacteria, is a central focus (Meyerholt et al., 2020; Peng et al., 2020; Stocker et al., 2016; Thomas et al., 2015; Wieder et al., 2015). BNF is the primary natural input of N to terrestrial ecosystems (Fowler et al., 2013; Vitousek et al., 2013). Symbiotic BNF, which occurs via symbioses between plants and N-fixing bacteria occupying plant root nodules, can respond dynamically to N limitation: plants can upregulate and downregulate symbiotic BNF when N-limited and non-N limited respectively (Menge et al., 2015). Most C-N coupled land models represent BNF phenomenologically using the empirical relationship of BNF with either net primary production or evapotranspiration (Davies-Barnard et al., 2020), which cannot represent the regulation of BNF by N limitation. A small number of recent C-N coupled land models incorporate a

mechanistic BNF representation, in which C allocation to symbiotic BNF is optimized to maximize plant growth, capturing the dynamic response of symbiotic BNF to N limitation, such as CABLE (Haverd et al., 2018; Peng et al., 2020; Wang et al., 2010), CLM5 (Lawrence et al., 2019), E3SM (Zhu et al., 2019), GFDL LM3-SNAP (Kou-Giesbrecht et al., 2021; Sulman et al., 2019), and O-CN (Meyerholt et al., 2020). In addition to regulating symbiotic BNF, plants can respond dynamically to N limitation by increasing C:N ratios (Elser et al., 2010; Meyerholt & Zaehle, 2015; Sistla & Schimel, 2012), by allocating C to mycorrhizae which secrete enzymes that accelerate the decomposition of soil organic matter (Phillips et al., 2013), and rhizosphere priming (primarily through root C exudation which stimulates the decomposition of soil organic matter; Cheng et al., 2014; Finzi et al., 2015), among others. These strategies modulate the extent to which N limitation constrains terrestrial C sequestration and their representation in land models would enable more realistic projections of the terrestrial C sink.

Global change drivers influence N limitation of plant growth and consequently representing the dynamic response of vegetation to N limitation is necessary to simulate the terrestrial C sink under global change. As the dominant natural input of N to terrestrial ecosystems, BNF plays an important role in regulating the response of vegetation to global change drivers (Terrer et al., 2018; Zheng et al., 2019, 2020): Symbiotic BNF has been observed to increase in response to elevated atmospheric CO_2 concentration (which intensifies N limitation ; Luo et al., 2004; Terrer et al., 2019) but decrease in response to elevated N deposition (which relieves N limitation ; Zheng et al., 2019, 2020). As global change drivers interact and amplify, projecting the terrestrial C sink under future global change requires a representation of the dynamic response of vegetation to N limitation in land models.

Here we present an analysis of terrestrial C and N cycling as regulated by the dynamic response of vegetation to N limitation over the historical period. We include a novel representation of BNF in the Canadian Land Surface Scheme Including Biogeochemical Cycles (CLASSIC) model (Melton et al., 2020; Seiler et al., 2021), which is the land component in the family of the Canadian Earth System Models (CanESM; Arora et al., 2009; Swart et al., 2019). CLASSIC recently adopted a representation of N cycling (Asaadi & Arora, 2021). We improve the previous static representation of BNF that is unresponsive to N limitation by implementing a representation of symbiotic BNF that is regulated by N limitation and thus responds to elevated atmospheric CO_2 concentration and elevated N deposition. In addition, we implement an independent representation of free-living BNF. We use CLASSIC to address the following questions: How do experimental manipulations of global change drivers (specifically, elevated CO_2 and N fertilisation) influence N limitation of plant growth, symbiotic BNF, and the dynamic response of vegetation to N limitation in comparison to observation-based estimates from meta-analyses? How have global change drivers (i.e., atmospheric CO_2 concentration, N deposition, climate, and land use change) over the historical period, individually and concurrently, influenced the dynamic response of vegetation to N limitation and the terrestrial C sink?

2 CLASSIC model structure and C-N cycle interactions

CLASSIC simulates land-atmosphere fluxes of energy, momentum, water, C, and N, and it can be run at a point, regional or global scale and at any spatial resolution. Here, a spatial resolution of 2.81˚C is used. A brief overview of physical processes and C biogeochemical processes in CLASSIC is provided in Section 2.1, and is described in detail in Melton et al., 2020; Seiler et al., 2021. An overview of N biogeochemical processes in CLASSIC is provided

in Section 2.2. These are described in detail in Asaadi & Arora, 2021. The new representation of the dynamic response of vegetation to N limitation of plant growth in CLASSIC, including BNF, is introduced in Section 2.3.

2.1 Overview of CLASSIC

2.1.1 Physical processes

The physical component of CLASSIC simulates fluxes of energy, momentum, and water at a 30 minute time step and evolved from the Canadian Land Surface Scheme (CLASS; Verseghy, 1991; Verseghy et al., 1993). The soil profile is represented by 20 soil layers, starting with 10 soil layers of 0.1 m thickness followed by soil layers of increasing thickness up to a soil layer of 30 m thickness for a total depth of over 61 m. The depth of permeable soil layers and thus the depth to bedrock soil layers varies geographically and is specified based on the SoilGrids250m data set (Hengl et al., 2017). Each grid cell is considered independent and there are no lateral transfers of energy, momentum, and water between grid cells.

2.1.2 Carbon biogeochemical processes

The biogeochemical component of CLASSIC simulates the land-atmosphere exchange of C via photosynthesis, autotrophic respiration and heterotrophic respiration, land use change, and fire and evolved from the Canadian Terrestrial Ecosystem Model (CTEM; Arora & Boer, 2005a). CLASSIC's photosynthesis equations are based on the standard biochemical model of photosynthesis in Collatz et al., 1991, 1992; Farquhar et al., 1980. Photosynthesis is simulated at a 30 minute time step similarly to the physical component of CLASSIC while all other biogeochemical processes are simulated at a daily time step. For biogeochemical processes, vegetation is partitioned into nine PFTs: needleleaf evergreen trees, needleleaf deciduous trees, broadleaf evergreen trees, broadleaf cold deciduous trees, broadleaf drought deciduous trees, C_3 crops, C_4 crops, C_3 grasses, and C_4 grasses. Figure S1 is a schematic illustration of the structure of the biogeochemical component of CLASSIC.

CLASSIC prognostically simulates the C pool in vegetation, litter, and soil organic matter for each PFT and over the bare soil fraction in each grid cell. Vegetation C is represented by three C pools: leaf, stem, and root (C_L, C_S, and C_R, respectively; kg C m^{-2}), each of which consists of structural and non-structural C pools. Litter and soil organic matter are represented by the litter C pool (C_D; kg C m^{-2}) and the soil organic C pool (C_H; kg C m^{-2}) respectively.

Photosynthesis generates non-structural carbohydrates which are allocated between the non-structural leaf, stem, and root C pools. Autotrophic respiration occurs from the non-structural leaf, stem, and root C pools (Arora & Boer, 2005a). Non-structural carbohydrates are converted to structural carbohydrates as C is transferred from the non-structural C pools to the structural C pools for each vegetation component (Asaadi et al., 2018).

Leaf, stem, and root turnover transfer C from the vegetation C pool to the to the litter C pool. In addition to normal leaf turnover, leaf turnover also occurs due to drought stress, cold stress, and shorter day lengths, affecting leaf phenology (Arora & Boer, 2005a). Land use change transfers C from the vegetation C pool to the litter C pool as well as the vegetation product pools, whereas fire emits C to the atmosphere and also transfers C from the vegetation C pool to the litter C pool (Arora & Boer, 2005b, 2010; Arora & Melton, 2018). C associated with

143 decomposing litter is transferred from the litter to the soil organic C pool. Finally, heterotrophic
144 respiration occurs from both the litter and soil organic C pools (Melton et al., 2015).

145 2.2 Nitrogen biogeochemical processes in CLASSIC

146 CLASSIC simulates the land-atmosphere exchange of N via BNF (free-living and
147 symbiotic), specified atmospheric N deposition and N fertiliser application, nitric oxide (NO)
148 emissions, nitrous oxide (N_2O) emissions, N_2 emissions, ammonia (NH_3) volatilisation, N
149 leaching, and land use change (Asaadi & Arora, 2021). Similar to C cycling, CLASSIC
150 prognostically simulates the N pool in vegetation, litter, soil organic matter, and inorganic soil N
151 for each PFT and over the bare soil fraction in each grid cell. Vegetation N is represented by
152 three N pools: leaf, stem, and root (N_L, N_S, and N_R, respectively; g N m^{-2}), each of which
153 consists of structural and non-structural N pools. Litter and soil organic matter are represented by
154 the litter N pool (N_D; g N m^{-2}) and the soil organic N pool (N_H; g N m^{-2}). Inorganic soil N is
155 represented by the soil NH_4^+ pool (N_{NH_4}; g N m^{-2}), and the soil NO_3^- pool (N_{NO_3}; g N m^{-2}). N
156 budget equations are described Text S1. Parameter values for new parameterisations are given in
157 Table S1.

158 N enters the soil-vegetation system via BNF, atmospheric N deposition, and N fertiliser
159 application. Atmospheric N deposition and N fertiliser application enter the soil NH_4^+ and NO_3^-
160 pools. In the previous static representation of BNF in CLASSIC, BNF was not separated into its
161 free-living and symbiotic components – it was represented as a function of soil temperature and
162 soil moisture that contributed to the soil NH_4^+ pool (Asaadi & Arora, 2021). In the new dynamic
163 representation of BNF in CLASSIC presented here, free-living and symbiotic BNF are calculated
164 separately. Free-living BNF contributes to the soil organic N pool and symbiotic BNF
165 contributes to the vegetation N pool. Root uptake of the soil NH_4^+ and NO_3^- pools occurs through
166 both the passive and active pathway. Together, root uptake of the soil NH_4^+ and NO_3^- pools and
167 symbiotic BNF are allocated between the non-structural leaf, stem, and root N pools. Similar to
168 C cycling, N is moved from the non-structural N pools to the structural N pools for each
169 vegetation component.

170 N demand of a given vegetation component is determined based on the fraction of net
171 primary productivity (NPP) allocated to that vegetation component divided by the minimum
172 prescribed C:N ratio for that vegetation component:

173 $$\Delta_i = \frac{\max(0, \alpha_i NPP)}{C{:}N_{i,min}}, i = L, S, R \quad (1)$$

174 where Δ_i is N demand of vegetation component i (g N m^{-2} day^{-1}), NPP is net primary
175 productivity (kg C m^{-2} day^{-1}), α_i is the fraction of NPP allocated to vegetation component i
176 (unitless), and $C{:}N_{i,min}$ is the minimum prescribed C:N ratio for vegetation component i (kg C g
177 N^{-1}). This assumes that vegetation attempts to achieve the minimum prescribed C:N ratio for all
178 vegetation components. N demand of vegetation (Δ_V; g N m^{-2} day^{-1}) is the sum of the N demand
179 of its components:

180 $$\Delta_V = \Delta_L + \Delta_S + \Delta_R \quad (2)$$

181 N allocation to a given vegetation component depends both on plant uptake of N and the
182 N demand of that vegetation component:

$$A_i = \begin{cases} \frac{\Delta_i}{\Delta_V}(U + B_s) & NPP > 0 \\ \frac{1}{C{:}N_{i,min}}(U + B_s) & NPP \leq 0 \end{cases}, i = L, S, R \quad (3)$$

where A_i is N allocation to vegetation component i (g N m^{-2} day^{-1}), U is root uptake of soil NH_4^+ and NO_3^- through both the passive and active pathway (g N m^{-2} day^{-1}) and B_s is symbiotic BNF (g N m^{-2} day^{-1}). When NPP is negative, such as for broadleaf cold deciduous trees during the winter, N allocation to a given vegetation component is determined based on its prescribed minimum C:N ratio. Because the C and N pools of each vegetation component are determined prognostically and independently, the C:N ratios for each vegetation component and thus the C:N ratio for vegetation evolve freely.

N processes associated with turnover and land use change follow the corresponding C processes. Leaf, stem, and root turnover transfer N from the vegetation N pool to the litter N pool. Land use change also transfers N from the vegetation N pool to the litter N pool, vegetation product pools, and atmosphere. N associated with decomposing litter is transferred from the litter to the soil organic N pool. The litter C:N ratio evolves freely driven by the C:N ratio for vegetation components. N mineralisation occurs from both the litter and soil matter N pools and contributes to the NH_4^+ pool. Opposing N mineralisation, N immobilization occurs from the NH_4^+ and NO_3^- pools and contributes to the soil organic N pool to maintain a prescribed C:N ratio of 13. Soil organic matter is the only pool in CLASSIC with a constant C:N ratio. Nitrification transfers N from the NH_4^+ pool to the NO_3^- pool and emits NO and N_2O. Denitrification transfers N from the NO_3^- pool to the atmosphere as N_2 and emits NO and N_2O as well. NH_3 volatilization transfers N from the NH_4^+ pool to the atmosphere as NH_3. N is leached from the NO_3^- pool.

Free-living BNF is represented as a function of temperature and soil organic C (which serves as a proxy for microbial biomass):

$$B_f = r_{BNF,f} f(\overline{T_k}) C_H \quad (4)$$

$r_{BNF,f}$ is a rate parameter for free-living BNF (g N kg C^{-1} day^{-1}), $f(\overline{T_k}) = \exp\left(-2.6 + 0.21\overline{T_k}\left(1 - \frac{0.5\overline{T_k}}{24.4}\right)\right)$ is the temperature dependence function from Houlton et al., 2008 (unitless), where $\overline{T_k}$ is average soil temperature across the soil layers in the top 50 cm (in which free-living BNF is assumed to occur) (˚C). Note that free-living BNF can also occur in other ecosystem niches, such as in bryophytes and lichens (Reed et al., 2011), which are not represented.

2.3 Dynamic response of vegetation to nitrogen limitation of plant growth in CLASSIC

Vegetation exhibits a dynamic response to N limitation of plant growth via three strategies in CLASSIC. First, vegetation upregulates and downregulates symbiotic BNF in response to weak N limitation and strong weak N limitation respectively. Second, vegetation modulates the C:N ratios for each vegetation component and thus the C:N ratio of vegetation in response to changing C and N supply. Finally, photosynthesis carboxylation capacity is dependent on leaf N such that, when leaf N is low, photosynthetic capacity is downregulated and, when leaf N is high, photosynthetic capacity is upregulated.

220 2.3.1 Symbiotic BNF

221 Symbiotic BNF is represented as a function of temperature and N stress of vegetation:

222 $$B_s = r_{BNF,s} \max\left(0, N_{stress} - b_{BNF,s}\right) f(T) \quad (5)$$

223 B_s is symbiotic BNF (g N m^{-2} day^{-1}), N_{stress} is N stress of vegetation (unitless, varies between 0
224 and 1), $r_{BNF,s}$ is a PFT-dependent BNF rate (g N m^{-2} day^{-1}), and $b_{BNF,s}$ is a parameter describing
225 the threshold N stress of vegetation above which symbiotic BNF occurs (unitless). $r_{BNF,s}$ for
226 crops is set greater than $r_{BNF,s}$ for natural PFTs and $b_{BNF,s} = 0$ for crops whereas $b_{BNF,s} > 0$ for
227 natural PFTs to account for the artificial selection of N-fixing crops over 4,000 years (O'Hara,
228 1998). $f(T) = \max\left(0, \left(\frac{44.83-T}{44.83-32.72}\right)\left(\frac{T-1.3}{32.72-1.3}\right)^{\frac{32.72-1.3}{44.83-32.72}}\right)$ is the temperature dependence
229 function from (Bytnerowicz et al., 2022) (unitless), where T is soil temperature of the top soil
230 layer (˚C). B_s as a function of varying N_{stress} (assuming constant T) is illustrated in Figure S2a.

231 N stress of vegetation is determined by N demand of vegetation relative to root uptake of
232 soil NH_4^+ and NO_3^-:

233 $$N_{stress} = \max\left(0, \min\left(\frac{\Delta_V - U}{\Delta_V}, 1\right)\right) \quad (6)$$

234 N_{stress} varies between 0 and 1. When root uptake of soil NH_4^+ and NO_3^- (U) meets or exceeds N
235 demand of vegetation (Δ_V), then $N_{stress} = 0$ indicating no N stress. When root uptake of soil
236 NH_4^+ and NO_3^- is zero, then $N_{stress} = 1$ indicating maximum N stress. When $0 < U < \Delta_V$ then
237 $0 < N_{stress} < 1$. N_{stress} as a function of varying Δ_V (assuming constant U) is illustrated in
238 Figure S2b.

239 Finally, the C cost of symbiotic BNF is a component of autotrophic respiration and is
240 added to maintenance respiration from the root C pool:

241 $$C_{BNF} = B_s \kappa \left[\frac{1}{1000}\right] \quad (7)$$

242 C_{BNF} is the C cost of symbiotic BNF (kg C m^{-2} day^{-1}), κ is the per unit C cost of symbiotic BNF
243 (assumed to be 6.5 g C g N^{-1} (Minchin & Witty, 2005)), and $\left[\frac{1}{1000}\right]$ converts the units from g C to
244 kg C.

245 Note that, in the previous static representation of BNF in CLASSIC, BNF was not
246 separated into its free-living and symbiotic components – it was represented as a function of soil
247 temperature and soil moisture that contributed to the soil NH_4^+ pool (Asaadi & Arora, 2021).

248 2.3.2 Vegetation C:N ratio

249 The C:N ratios for each vegetation component and thus the C:N ratio of vegetation
250 evolve freely in response to changing C and N supply. N demand of a given vegetation
251 component depends on its prescribed minimum C:N ratio (Equations 1 and 3). When C supply is
252 high relative to N supply, vegetation component C:N ratios increase, whereas, when C supply is
253 low relative to N supply, vegetation component C:N ratios decrease. Additionally, prescribed
254 maximum vegetation component C:N ratios as well as the leaf N pool are used to calculate
255 photosynthetic capacity (Section 2.3.3).

The prescribed minimum and maximum leaf C:N ratios are based on Kerkhoff et al., 2006; McGroddy et al., 2004, minimum and maximum stem C:N ratios are based on Weedon et al., 2009, and minimum and maximum root C:N ratios are based on Yuan et al., 2011.

2.3.3 Photosynthetic capacity downregulation

Maximum rate of carboxylation is a function of leaf N:

$$V_{cmax} = \Lambda\left(\Gamma_1 \frac{N_L}{LAI} + \Gamma_2\right) \quad (8)$$

V_{cmax} is the maximum rate of carboxylation (μmol CO_2 m^{-2} sec^{-1}), Λ describes the reduction in V_{cmax} when current vegetation component C:N ratios exceed prescribed maximum C:N ratios (unitless), Γ_1 is a PFT-dependent parameter from Kattge et al., 2009 (μmol CO_2 g N^{-1} sec^{-1}), LAI is leaf area index (m^2 m^{-2}), and Γ_2 is a PFT-dependent parameter from Kattge et al., 2009 (μmol CO_2 m^{-2} sec^{-1}). Note that, previously in Asaadi & Arora, 2021, Γ_1, Γ_2, and LAI were assumed to be global constants. Here, Γ_1 and Γ_2 are PFT-dependent parameters and LAI is simulated prognostically for each PFT.

The reduction in V_{cmax} when current vegetation component C:N ratios exceed prescribed maximum C:N ratios is determined by the difference in current C:N ratio to prescribed maximum C:N ratio for all vegetation components:

$$\Lambda = \exp\left(-k_\Lambda\left(\sum_i \frac{{}^1/_{C:N_{i,max}}}{\sum_i {}^1/_{C:N_{i,max}}} \max\left(0, C{:}N_i - C{:}N_{i,max}\right)\right)\right) \quad (9)$$

k_Λ is a parameter describing the strength of the reduction in V_{cmax} when $C{:}N_i$ exceeds $C{:}N_{i,max}$ (unitless), $C{:}N_i$ is the current C:N ratio of vegetation component i (kg C g N^{-1}), and $C{:}N_{i,max}$ is the maximum C:N ratio of vegetation component i (kg C g N^{-1}). Λ varies between 0 and 1. When $C{:}N_i$ do not exceed $C{:}N_{i,max}$ for all vegetation components, $\Lambda = 1$ indicating no reduction in V_{cmax}. When $C{:}N_i$ exceeds $C{:}N_{i,max}$ for some or all vegetation components, $0 < \Lambda < 1$ and V_{cmax} is reduced. This provides a feedback that reduces photosynthetic capacity further than would be obtained from only the reduction in N_L in Equation 8 when the current vegetation C:N ratio is high.

3 Methodology

3.1 CLASSIC simulations and forcing data sets

The simulations performed for this study used atmospheric CO_2 concentration, meteorological, population density, land use change, N deposition, and N fertilisation forcings based on the TRENDY protocol for 2019 and are described in Text S2. Annual TRENDY simulations contribute to the Global Carbon Project (Friedlingstein et al., 2019). We first performed a pre-industrial spin up using atmospheric CO_2 concentration, population density, land cover, N deposition, and N fertilisation forcings corresponding to the year 1700. In the absence of meteorological forcing before 1901, we used meteorological forcing from 1901 to 1925 repeatedly until the C and N pools came into equilibrium. Thresholds of 0.05 Pg C yr^{-1} for the global net atmosphere-land CO_2 flux and 0.5 Tg N yr^{-1} for the global net atmosphere-land N flux were used to assess if equilibrium was achieved.

We launched two sets of simulations with initial conditions from the pre-industrial spin up. The first set of simulations consist of elevated CO_2 and N fertilisation experiments. For these simulations, we followed the protocol outlined in Davies-Barnard et al., 2020, allowing the comparison of our simulations to their results. First, we simulated the period from 1701 to 1995 (using meteorological forcing from 1901 to 1925 repeated eight times for the period from 1701 to 1900). Then, for the period from 1996 to 2015, we simulated an instantaneous 200 ppm increase in CO_2 relative to normal historical CO_2 values. Similarly, we simulated an instantaneous 50 kg N ha^{-1} yr^{-1} increase in N deposition relative to normal historical N deposition values. Finally, we simulated the period from 1996 to 2015 with normal historical CO_2 and N deposition values. All other forcings (meteorological, population density, land cover, and N fertilisation) for the period from 1996 to 2015 follow their normal historical values. The effects of elevated CO_2 and N fertilisation were calculated by differencing the results from the elevated CO_2 and N fertilisation experiments over the period from 1996 to 2015 with the results from the simulation with normal historical CO_2 and N deposition values over the period from 1996 to 2015.

The second set of simulations consist of historical simulations for the period from 1701 to 2018 in which we examined the effect of global change drivers concurrently and individually. The global change drivers that we examined are atmospheric CO_2 concentration, N deposition, climate, and land use change (which is characterized by changing crop area and N fertiliser application) (Figure 1). Table S2 describes the forcings for each simulation. Note that, because population density only affects fire and the overall effect of fire on C cycling is much smaller than those of other global change drivers, we do not evaluate the population density forcing individually and it follows its normal historical values in all simulations.

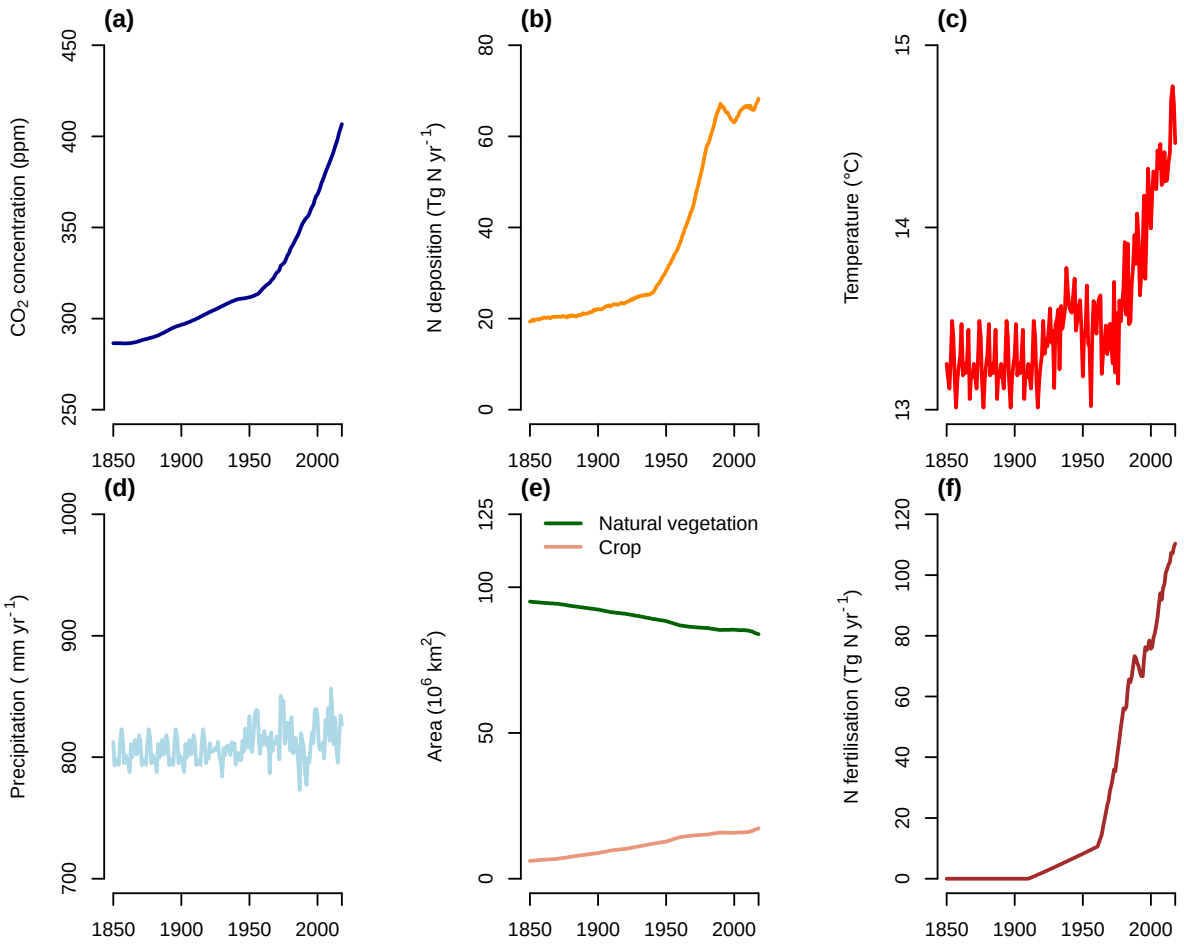

316

317 **Figure 1.** Globally-averaged values of the studied global change drivers over the period from
318 1701 to 2018. (a) Atmospheric CO_2 concentration. (b) N deposition. (c) Temperature. (d)
319 Precipitation. (e) Global land area covered by natural vegetation and crops. (f) N fertiliser
320 application.

We conducted all simulations with three versions of CLASSIC. The first version, CLASSIC, is the standard land model with coupled C and N cycling. The second version, CLASSIC-statN, is a modification of CLASSIC in which the regulation of BNF by N limitation is turned off. While in CLASSIC symbiotic BNF is a function of time-evolving N_{stress} (Equation 5), in CLASSIC-statN symbiotic BNF is represented as a function of temperature and the globally-averaged N_{stress} over the pre-industrial spin up (0.1):

$$B_s = r_{BNF,s} f(T)(0.1) \quad (10)$$

As a result, symbiotic BNF in CLASSIC-statN is unresponsive to changes in N_{stress} that are associated with changing N limitation.

The third version, CLASSIC-C, has N cycling turned off and the downregulation of photosynthetic capacity due to N limitation under elevated atmospheric CO_2 concentration is controlled by an empirical parameter as explained in Arora et al., 2009; Asaadi & Arora, 2021. Briefly, this empirical parameter, which ranges between 0 and 0.9, determines the rate of increase of photosynthesis with increasing atmospheric CO_2 concentration. When it is set to 0, photosynthesis does not increase with increasing atmospheric CO_2 concentration. When it is set to 0.9, photosynthesis increases with increasing atmospheric CO_2 concentration at an unconstrained rate that is determined by CLASSIC's photosynthesis equations which are based on the standard biochemical model of photosynthesis in Collatz et al., 1991, 1992; Farquhar et al., 1980. Here, we set this empirical parameter to 0.35 to yield a global net atmosphere-land CO_2 flux that lies within the uncertainty range of estimates from the Global Carbon Project (Friedlingstein et al., 2019). The uncertainty associated with this empirical parameter and this representation of the downregulation of photosynthetic capacity due to N limitation under elevated atmospheric CO_2 concentration motivated the implementation of coupled C and N cycling in CLASSIC (Asaadi & Arora, 2021).

3.2 Evaluation

We compared simulated C and N pools and fluxes to observation-based estimates (Beer et al., 2010; Davies-Barnard & Friedlingstein, 2020; Fowler et al., 2013; Friedlingstein et al., 2019; Herridge et al., 2008; Köchy et al., 2015; Martens et al., 2017; Vitousek et al., 2013; Xu et al., 2021). We compared the globally-averaged response of simulated NPP to elevated CO_2 (+200 ppm) and N fertilisation (+50 kg N ha^{-1} yr^{-1}) against estimates from (Song et al., 2019), which is a meta-analysis of manipulative experiments that recorded how NPP responds to global change drivers. We compared the globally-averaged response of simulated BNF to elevated CO_2 (+200 ppm) against estimates from (Liang et al., 2016), a meta-analysis of manipulative experiments that recorded how BNF responds to elevated CO_2. We compared the globally-averaged response of simulated BNF to N fertilisation (+50 kg N ha^{-1} yr^{-1}) against estimates from (Zheng et al., 2019), a meta-analysis of manipulative experiments that recorded how BNF responds to N fertilisation. We used results for natural ecosystems from the dataset in (Liang et al., 2016), whereas (Song et al., 2019) and (Zheng et al., 2019) report results for natural ecosystems exclusively. We also compared the response of NPP and BNF to elevated CO_2 and N fertilisation in CLASSIC simulations to results from five CMIP6 (Coupled Model Intercomparison Project Phase 6; Eyring et al., 2016) land models described in (Davies-Barnard et al., 2020) – the Community Land Model version 4.5 (CLM4.5), the Community Land Model version 5 (CLM5), the JSBACH version 3.20 model, the Joint UK Land Environment Simulator version 5.4 (JULES-ES), and the Lund-Potsdam-Jena General Ecosystem Simulator version 4.0

(LPJ-GUESS). These land models represent coupled C and N cycling and implement different representations of key N cycling processes, including their representation of BNF (Table S3). Note that, among these land models, CLM5 is the only land model that distinguishes between free-living and symbiotic BNF and that captures the regulation of BNF by N limitation.

4 Results and discussion

4.1 BNF evaluation

CLASSIC reproduces global pre-industrial total BNF (free-living and symbiotic), present-day free-living BNF, present-day natural symbiotic BNF, and present-day crop BNF reasonably well in comparison to observation-based estimates and other CMIP6 land models (Figure 2). CLASSIC simulates 64 Tg N yr^{-1} for pre-industrial total BNF, which is comparable to estimates of 58 Tg N yr^{-1} (40 – 100 Tg N yr^{-1}) from (Vitousek et al., 2013). Simulated present-day free-living BNF (23 Tg N yr^{-1}) and present-day natural symbiotic BNF (47 Tg N yr^{-1}) are also comparable to estimates of 31 Tg N yr^{-1} (21 – 66 Tg N yr^{-1}) and 57 Tg N yr^{-1} (31 – 66 Tg N yr^{-1}), respectively, from (Davies-Barnard & Friedlingstein, 2020). As such, CLASSIC simulates 70 Tg N yr^{-1} for present-day natural BNF (combined free-living and natural symbiotic). This is similar to estimates from CLM4.5, CLM5, JSBACH, JULES-ES, and LPJ-GUESS, which range from 46 to 107 Tg N yr^{-1} (Table S4), as well as to other CMIP6 land models, such as 73 – 122 Tg N yr^{-1} by CABLE (Peng et al., 2020) and 37 – 117 Tg N yr^{-1} by O-CN (Meyerholt et al., 2020). Simulated present-day crop symbiotic BNF (74 Tg N yr^{-1}) is comparable to estimates of 50 – 70 Tg N yr^{-1} from (Herridge et al., 2008).

Free-living BNF is greatest in tropical biomes (Figure 2d) due to higher temperatures. Natural symbiotic BNF is greatest in tropical biomes (Figure 2e), as expected (Hedin et al., 2009). Natural symbiotic BNF is higher in tropical America than in tropical Africa and Asia, corresponding to higher N deposition in tropical Africa and Asia (Figure S3) which relieves N limitation. Crop symbiotic BNF is greatest in regions with high crop area (Figure 2f, Figure S4).

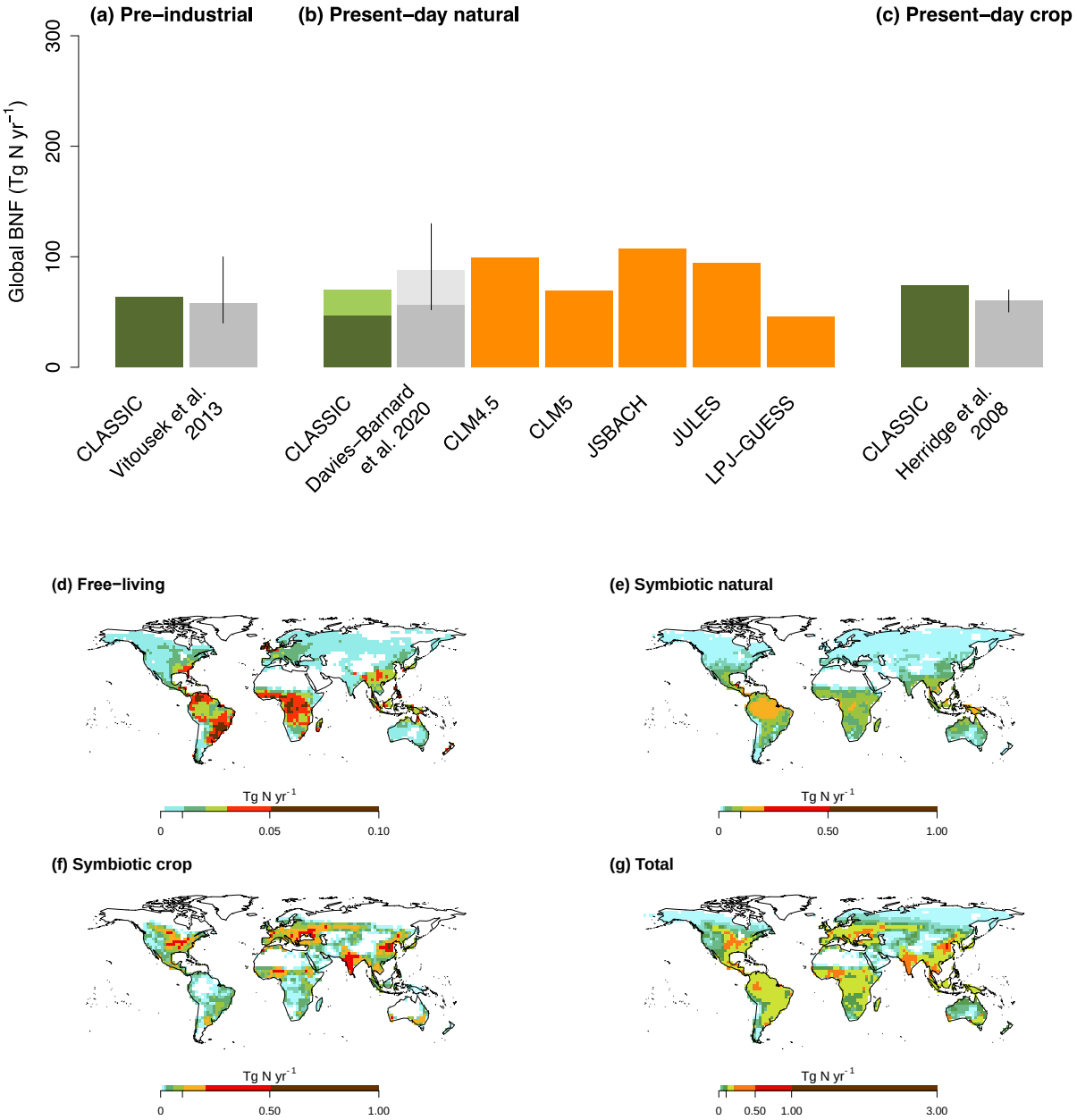

Figure 2. Biological nitrogen fixation simulated by CLASSIC, observation-based estimates from Davies-Barnard & Friedlingstein, 2020; Herridge et al., 2008; Vitousek et al., 2013, and estimates from other CMIP6 land models (CLM4.5, CLM5, JSBACH, JULES-ES, and LPJ-GUESS; Davies-Barnard et al., 2020). (a) Global pre-industrial biological nitrogen fixation (averaged over 1701 to 1721). (b) Global present-day natural biological nitrogen fixation (averaged over 1998 to 2018). When free-living and natural symbiotic biological nitrogen fixation are differentiated, they are distinguished by lighter and darker colours respectively. (c) Global present-day crop symbiotic biological nitrogen fixation (averaged over 1998 to 2018). Geographical distribution of present-day (d) free-living biological nitrogen fixation, (e) natural symbiotic biological nitrogen fixation, and (f) crop symbiotic biological nitrogen fixation (averaged over 1998 to 2018).

Few land models incorporate an explicit representation of free-living BNF, combining it with natural symbiotic BNF. However, observations suggest that free-living BNF may be a substantial N input to terrestrial ecosystems. Reed et al., 2011 suggests that free-living BNF rates are comparable to natural symbiotic BNF rates in some terrestrial ecosystems. Elbert et al., 2012 suggests that cryptogamic covers (N-fixing photoautotrophic communities that cover terrestrial surfaces) account for 49 Tg N yr^{-1}, while Davies-Barnard & Friedlingstein, 2020 suggests that global free-living BNF is 31 Tg N yr^{-1} (21 – 66 Tg N yr^{-1}) and contributes ~35% of natural BNF. Because free-living BNF is not directly influenced by N limitation, its distinction from natural symbiotic BNF is important for representing the dynamic response of vegetation to N limitation.

4.2 Elevated CO_2 and N fertilisation experiments

4.2.1 NPP response to elevated CO_2 and N fertilisation

The NPP response to elevated CO_2 (+200 ppm) simulated by CLASSIC was +11.3%, which is consistent with observation-based estimates (+15.6%; Song et al., 2019) (Figure 3a). This estimate also lies in the range of other CMIP6 land models (+5 to +20%; Davies-Barnard et al., 2020). The NPP response to N fertilisation (+50 kg N ha^{-1} yr^{-1}) simulated by CLASSIC was +16.1%, which is higher than observation-based estimates (+6.5%; Song et al., 2019) (Figure 3c). Other CMIP6 land models overestimated (CLM4.5, CLM5, and LPJ-GUESS) or underestimated (JSBACH and JULES) the NPP response to N fertilisation (Davies-Barnard et al., 2020).

CLASSIC-statN had a lower NPP response to elevated CO_2 (+7.5%) than that of CLASSIC because BNF is not upregulated in response to stronger N limitation due to elevated CO_2 in CLASSIC-statN. Similarly, CLASSIC-statN had a higher NPP response to N fertilisation (+20.8%) than that of CLASSIC because BNF is not downregulated in response to weaker N limitation due to N fertilisation in CLASSIC-statN. CLASSIC-C had a higher NPP response to elevated CO_2 (+22.7%) than that of CLASSIC. CLASSIC-C had no response to N fertilisation because there is no N limitation.

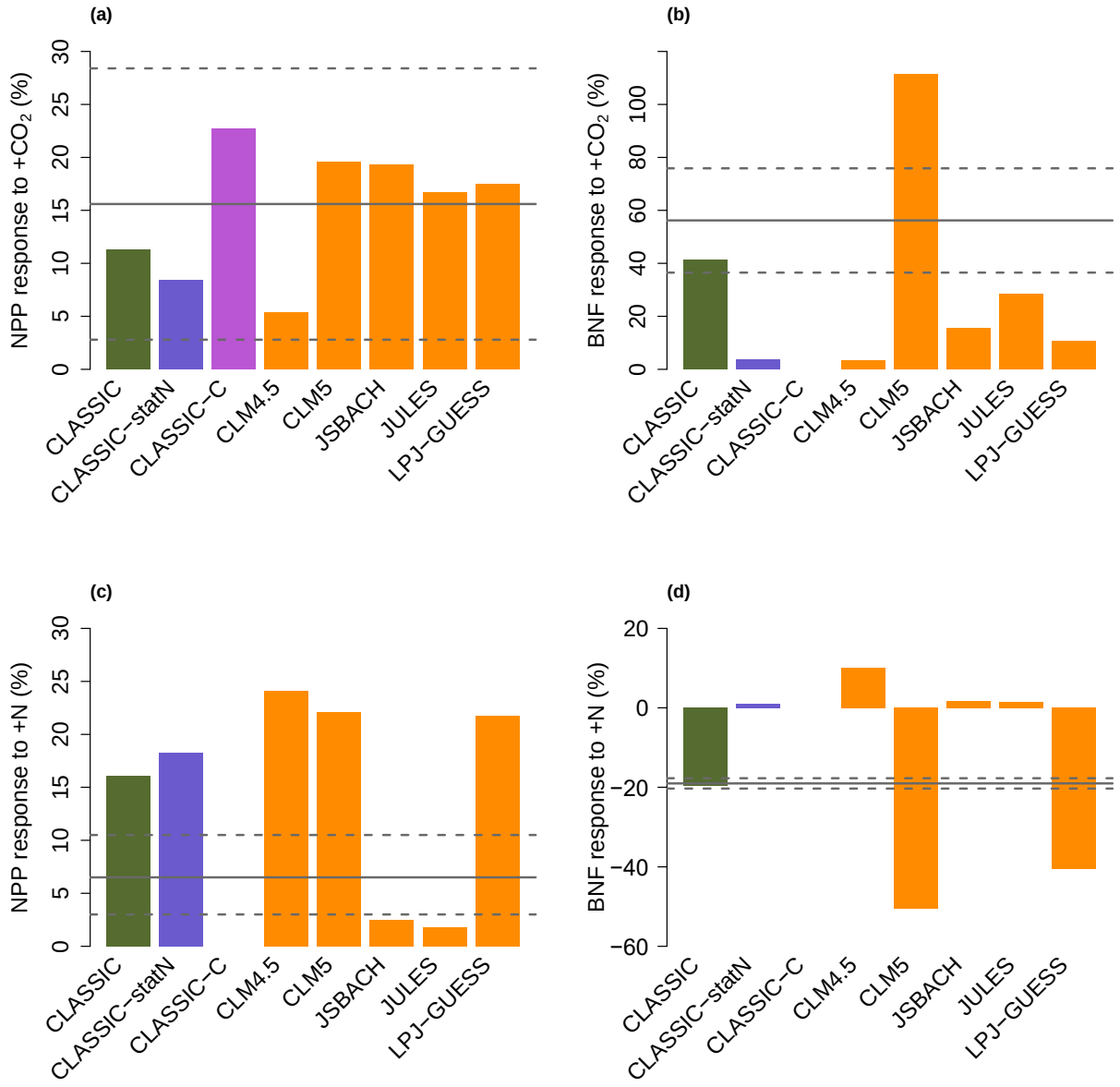

Figure 3. Response of (a) net primary productivity to elevated CO_2 (+200 ppm), (b) biological nitrogen fixation to elevated CO_2 (+200 ppm), (c) net primary productivity to nitrogen fertilisation (+50 kg N ha^{-1} yr^{-1}), and (d) biological nitrogen fixation to nitrogen fertilisation (+50 kg N ha^{-1} yr^{-1}) simulated by CLASSIC, CLASSIC without the regulation of BNF by N limitation (CLASSIC-statN), and CLASSIC without N cycling (CLASSIC-C). These estimates are compared to estimates from other CMIP6 land models (CLM4.5, CLM5, JSBACH, JULES, and LPJ-GUESS) and observation-based estimates from meta-analyses (indicated by the gray horizontal lines where the solid line indicates the mean and the dashed lines indicate the 95% confidence intervals). Observation-based estimates for the response of net primary productivity are from (Song et al., 2019), observation-based estimates for the response of biological nitrogen fixation to elevated CO_2 are from (Liang et al., 2016), and observation-based estimates for the

response of biological nitrogen fixation to nitrogen fertilisation (+50 kg N ha^{-1} yr^{-1}) are from (Zheng et al., 2019). Results are averaged over 1996 to 2015.

The response of NPP to elevated CO_2 decreases with increasing absolute latitude. Individual grid cells exhibit a lower NPP response to elevated CO_2 with increasing absolute latitude (Figure 4a; $P < 0.001$). This is due to the temperature dependence of photosynthesis which implies that the response of NPP to elevated CO_2 is stronger at higher temperatures consistent with observations (Baig et al., 2015; Long, 1991). Additionally, because the growing season is longer at lower latitudes than at higher latitudes, the response of NPP to elevated CO_2 is realised over a longer period at lower latitudes than at higher latitudes.

In contrast, the response of NPP to N fertilisation increases with increasing absolute latitude. Individual grid cells exhibit a higher NPP response to N fertilisation with increasing absolute latitude (Figure 4b; $P < 0.001$). Examining the response of NPP to N fertilisation allows for the assessment of N limitation (Sullivan et al., 2014). Higher latitude vegetation is suggested to be more N-limited than lower latitude vegetation (Brookshire et al., 2012; Du et al., 2020; LeBauer & Treseder, 2008). CLASSIC simulates a significantly stronger response to N fertilisation at high latitudes than at low latitudes, suggesting stronger N limitation at high latitudes than at low latitudes (Figure 4b). Thus, the stronger response to elevated CO_2 at low latitudes than at high latitudes is not only driven by the temperature dependence of photosynthesis (as described above) but also occurs because low latitudes are less N-limited than high latitudes. This causes the bimodality of the response of NPP at the grid cell scale, i.e., that NPP of a given grid cell tends to respond to either elevated CO_2 or to N fertilisation but not to both elevated CO_2 and N fertilisation (Figure 4c). This behaviour is consistent with that of other CMIP6 land models (Davies-Barnard et al., 2020).

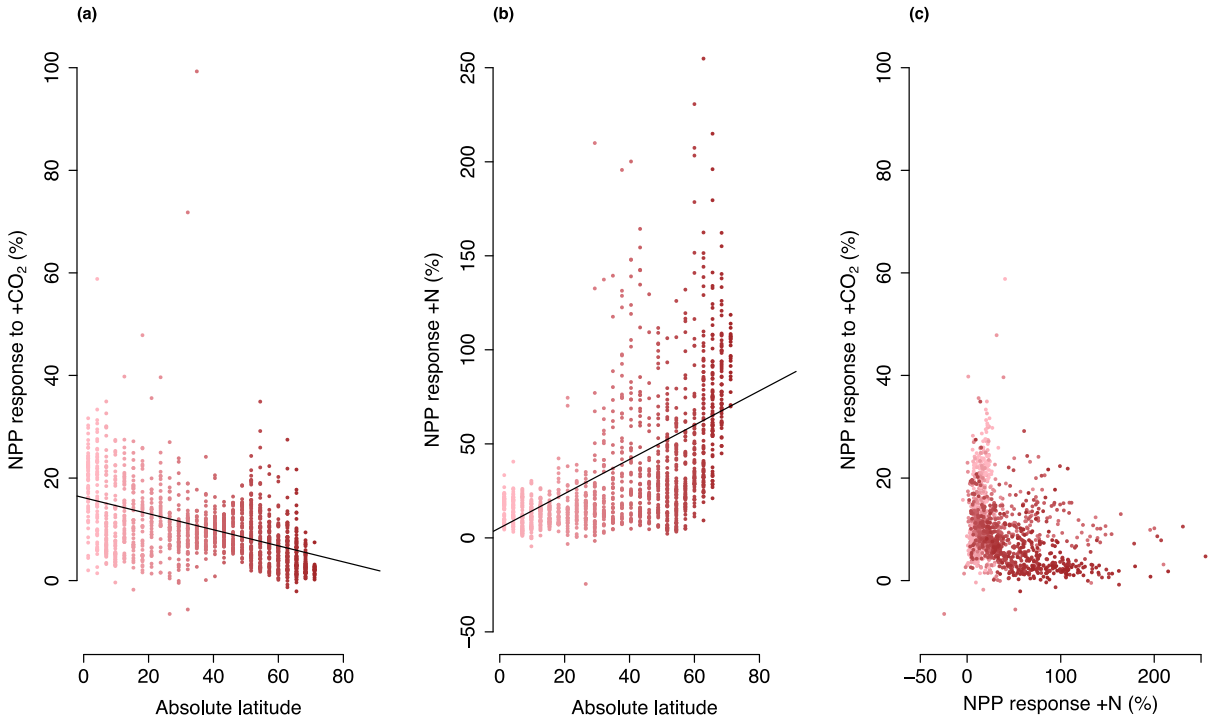

Figure 4. Responses of net primary productivity to elevated CO_2 (+200 ppm) and nitrogen fertilisation (+50 kg N ha^{-1} yr^{-1}) at the grid cell scale. (a) Response of net primary productivity to elevated CO_2 simulated by CLASSIC as a function of absolute latitude. (b) Response of net primary productivity to nitrogen fertilisation simulated by CLASSIC as a function of absolute latitude. (c) Net primary productivity response to both elevated CO_2 and nitrogen fertilisation simulated by CLASSIC. Each point represents an individual grid cell. Lighter colours represent lower latitudes and darker colours represent higher latitudes. Results are averaged over 1996 to 2015.

473 4.2.2 BNF response to elevated CO_2 and N fertilisation

474 The BNF response to elevated CO_2 (+200 ppm) simulated by CLASSIC was +41.4%,
475 which is consistent with observation-based estimates (+56.2%; Liang et al., 2016) (Figure 3b).
476 This is a more accurate response than other CMIP6 land models, which all lie outside this range:
477 CLM5 overestimated the BNF response to elevated CO_2 and CLM4.5, JSBACH, JULES-ES and
478 LPJ-GUESS underestimated the BNF response to elevated CO_2 (Davies-Barnard et al., 2020).
479 The BNF response to N fertilisation (+50 kg N ha^{-1} yr^{-1}) simulated by CLASSIC was –19.7%,
480 which is consistent with observation-based estimates (–19%; Zheng et al., 2019) (Figure 3d).
481 Other CMIP6 land models either overestimated (CLM5, and LPJ-GUESS) or underestimated
482 (CLM4.5, JSBACH, and JULES) the BNF response to N fertilisation (Davies-Barnard et al.,
483 2020).

484 The BNF response in CLASSIC is regulated by N limitation (represented as N stress in
485 Equations 5 and 6), which increases under elevated CO_2 and decreases under N fertilisation in
486 comparison to estimates from under normal historical CO_2 and N deposition values (Figure 5a).
487 This follows observations that elevated CO_2 intensifies N limitation (Luo et al., 2004), whereas
488 N fertilisation relieves N limitation (LeBauer & Treseder, 2008).

489 4.2.3 Overall response to elevated CO_2 and N fertilisation

490 In comparison to other CMIP6 land models (Davies-Barnard et al., 2020), CLM5 is the
491 sole other land model represented BNF regulation by N limitation (Table S3); CLM4.5,
492 JSBACH, JULES-ES and LPJ-GUESS represent BNF with empirical relationships between BNF
493 and NPP (CLM4.5, JSBACH, and JULES-ES) or BNF and ET (LPJ-GUESS). Similar to
494 CLASSIC, CLM5 estimated the expected directions of the BNF response to elevated CO_2 and N
495 fertilisation (i.e., increase and decrease) but overestimated BNF change under both elevated CO_2
496 and N fertilisation, whereas CLASSIC underestimated BNF change under N fertilisation (Figure
497 3).

498 In addition to regulating symbiotic BNF, plants can respond dynamically to N limitation
499 by increasing vegetation component C:N ratios (Elser et al., 2010; Sistla & Schimel, 2012).
500 Elevated CO_2 can increase the vegetation C:N ratio due to stimulated photosynthesis. N
501 fertilisation can decrease the vegetation C:N ratio due to "luxury" uptake of N. As such,
502 representing a flexible vegetation C:N ratio in land models results in the greatest agreement with
503 observations (Meyerholt & Zaehle, 2015). In CLASSIC, vegetation C:N ratio increases under
504 elevated CO_2 and decreases under N fertilisation in comparison to estimates from under normal
505 historical CO_2 and N deposition values (Figure 5b).

506 Having established confidence in CLASSIC's response to elevated CO_2 and N
507 fertilisation experiments we now evaluate CLASSIC's response to global change drivers over the
508 historical period.

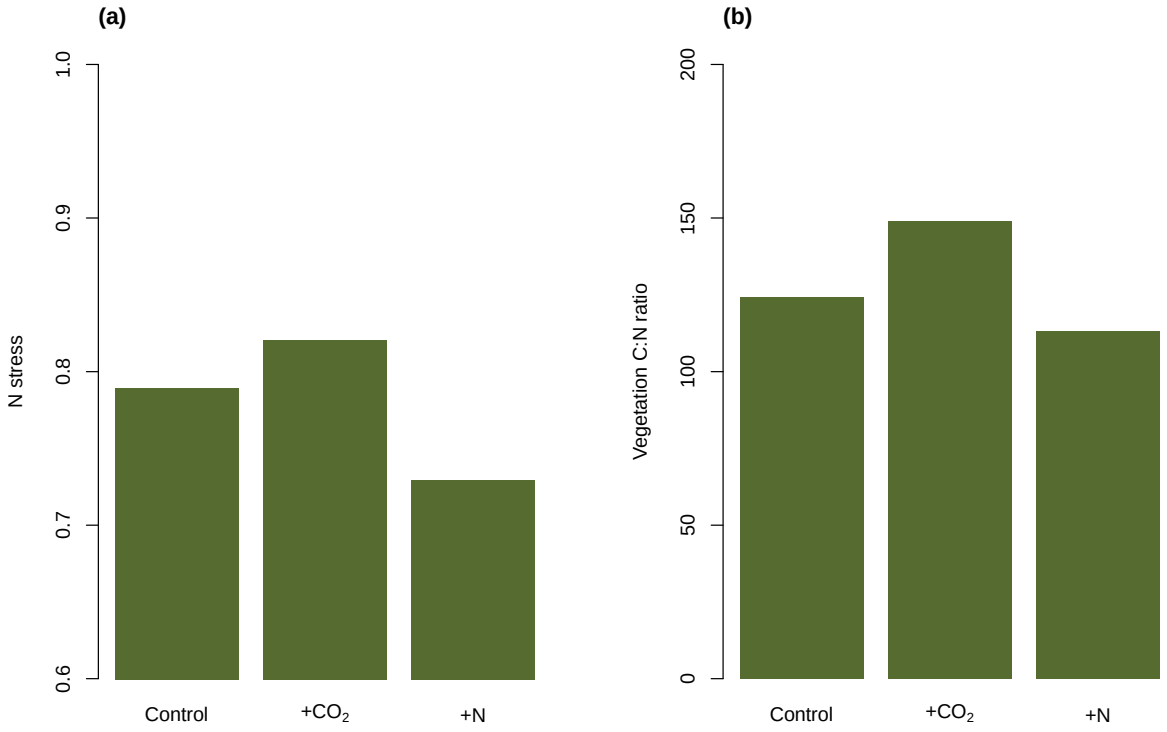

509

510 **Figure 5.** (a) Nitrogen stress and (b) vegetation carbon to nitrogen ratio under elevated CO_2
511 (+200 ppm) and under nitrogen fertilisation (+50 kg N ha^{-1} yr^{-1}) simulated by CLASSIC. These
512 estimates are compared to estimates under normal historical CO_2 and nitrogen deposition values
513 (control) simulated by CLASSIC. Results are averaged over 1996 to 2015.

4.3 Historical simulations

4.3.1 Individual global change drivers over the historical period

Similar to their responses in the elevated CO_2 experiment (+200 ppm CO_2), NPP and natural symbiotic BNF increase in the simulation driven with atmospheric CO_2 concentration acting in isolation over the historical period (Figure 6ab). NPP increases because elevated atmospheric CO_2 concentration stimulates photosynthesis (Collatz et al., 1991, 1992; Farquhar et al., 1980), i.e., CO_2 fertilisation (Walker et al., 2020). The increase in natural symbiotic BNF is due to an increase in N stress (Figure 6d). This follows observations that increased atmospheric CO_2 concentration intensifies N limitation (Luo et al., 2004; Terrer et al., 2019). Vegetation C:N ratio also increases due to increased C supply (Figure 6e) consistent with observations (Elser et al., 2010; Sistla & Schimel, 2012). Including N cycling reduces the NPP change when atmospheric CO_2 concentration is acting in isolation over the historical period: the NPP change for CLASSIC (5.6 Pg C yr^{-1}) is 45% that of CLASSIC-C (12.4 Pg C yr^{-1}). Furthermore, when BNF is not regulated by N limitation, the NPP change when atmospheric CO_2 concentration is acting in isolation over the historical period is even lower: the NPP change for CLASSIC-statN (3.5 Pg C yr^{-1}) is 28% that of CLASSIC-C (12.4 Pg C yr^{-1}).

Similar to their responses in the N fertilisation experiment (+50 kg N ha^{-1} yr^{-1}), NPP increases slightly and natural symbiotic BNF decreases slightly in the simulation driven with N deposition acting in isolation over the historical period (Figure 6ab). NPP increases because elevated N deposition stimulates photosynthesis by increasing leaf N (Equations 8 and 9). The decrease in natural symbiotic BNF is due to a decrease in N stress (Figure 6d). This follows observations that increased N deposition relieves N limitation (LeBauer & Treseder, 2008). The changes in NPP and natural symbiotic BNF are low in comparison to those from the N fertilisation experiment because the globally-averaged change in N deposition over the historical period (+1.6 kg N ha^{-1} yr^{-1} between pre-industrial and present-day values) is much lower than the N fertilisation treatment (+50 kg N ha^{-1} yr^{-1}).

Both NPP and natural symbiotic BNF increase slightly in the simulation driven with climate acting in isolation over the historical period (Figure 6ab). NPP increases, first, because elevated temperature stimulates photosynthesis and increases the length of the growing season and, second, because elevated precipitation relieves water limitation (although change in precipitation over the historical period is geographically variable with some regions experiencing increased precipitation and other regions experiencing decreased precipitation (Lau et al., 2013)). Additionally, elevated temperature and precipitation stimulate N mineralisation (Figure S5) which stimulates photosynthesis by increasing leaf N (Equations 8 and 9). The increase in natural symbiotic BNF occurs despite a slight decrease in N stress (Figure 6d). This slight decrease in N stress is likely due to elevated N mineralisation which overcomes the influence of elevated temperature and precipitation on stimulating photosynthesis, increasing the length of the growing season, and relieving water limitation which would all cause an increase in N stress. Given these counteracting drivers, the change in N stress is minimal. The increase in natural symbiotic BNF is thus due to elevated temperature because symbiotic BNF is a function of temperature as well as N stress (Equation 6).

In the simulation driven with land use change acting in isolation over the historical period (which includes both changing crop area and N fertiliser application), NPP increases and crop symbiotic BNF increases but natural symbiotic BNF decreases (Figure 6ac). This is due to higher

558 photosynthetic capacity of crops than of natural vegetation (Table S1; Kattge et al., 2009),
559 increasing crop area, and decreasing natural vegetation area, respectively. Note that the increase
560 in crop symbiotic BNF occurs because increasing crop area more than compensates for
561 increasing N fertiliser application which decreases N stress of crops.

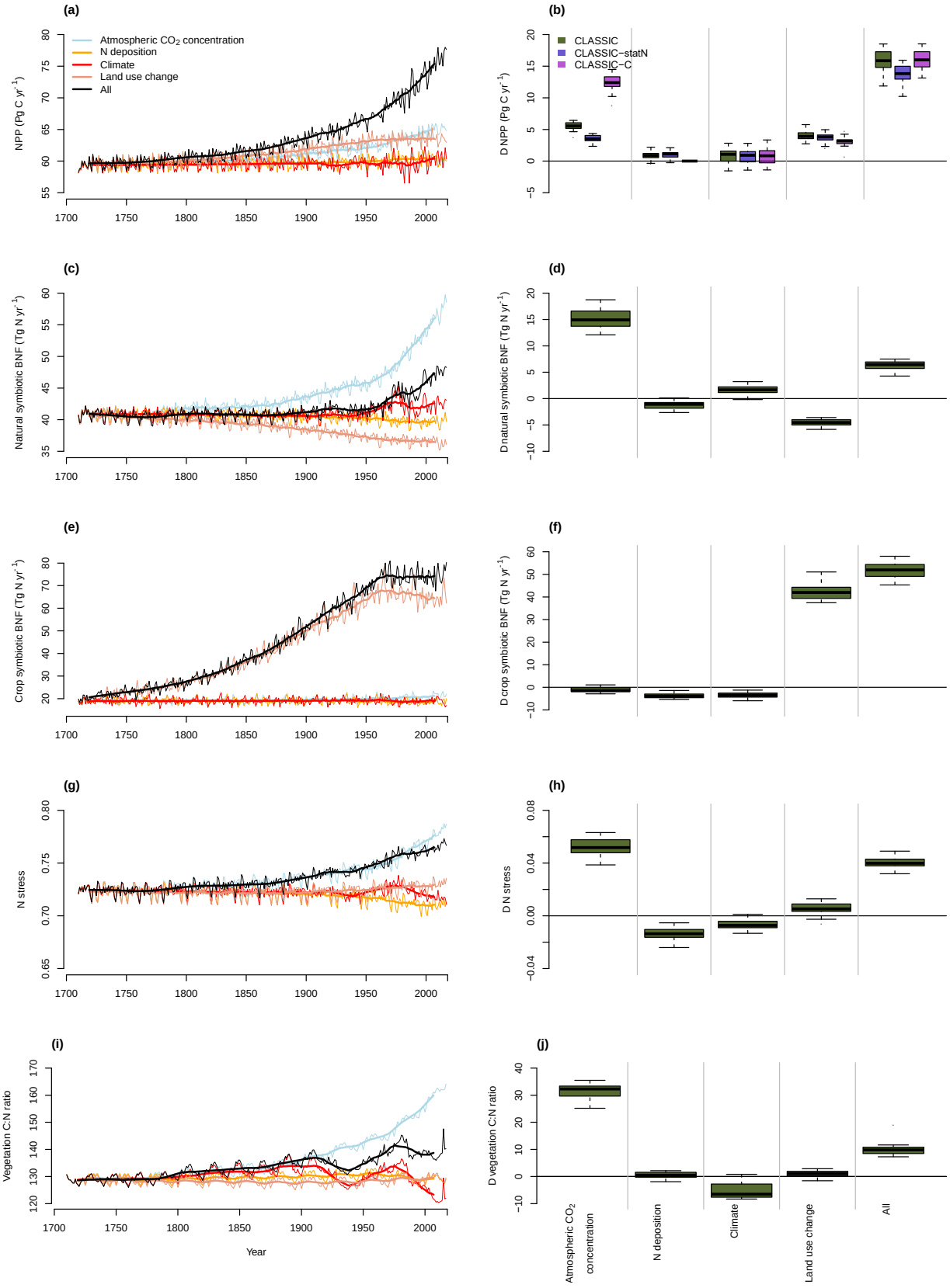
(a)
Atmospheric CO2 concentration
N deposition
Climate
Land use change
All
NPP (Pg C yr-1)
(b)
CLASSIC
CLASSIC−statN
CLASSIC−C
D NPP (Pg C yr-1)
(c)
Natural symbiotic BNF (Tg N yr-1)
(d)
D natural symbiotic BNF (Tg N yr-1)
(e)
Crop symbiotic BNF (Tg N yr-1)
(f)
D crop symbiotic BNF (Tg N yr-1)
(g)
N stress
(h)
D N stress
(i)
Vegetation C:N ratio
Year
(j)
D vegetation C:N ratio
Atmospheric CO2 concentration
N deposition
Climate
Land use change
All

563 **Figure 6.** Net primary productivity, symbiotic biological nitrogen fixation, nitrogen stress, and
564 vegetation carbon to nitrogen ratio over the historical period simulated by CLASSIC, CLASSIC
565 without the regulation of BNF by N limitation (CLASSIC-statN), and CLASSIC without N
566 cycling (CLASSIC-C) for all global change drivers concurrently and individually. (a), (c), (e)
567 and (g). Time series simulated by CLASSIC. (b), (d), (f), and (h). Change from pre-industrial
568 (averaged over 1701 to 1721) to present-day (1998 to 2018) estimates simulated by CLASSIC,
569 CLASSIC-statN, and CLASSIC-C (where the solid line indicates the median and the box extends
570 from the first quartile to the third quartile).

571 4.3.2 All global change driver concurrently over the historical period

572 CLASSIC reproduces observation-based estimates for global C and N pools and fluxes in
573 the historical simulation when all global change drivers are acting concurrently, similarly to
574 CLASSIC-C. CLASSIC reproduces the latitudinal patterns of GPP, vegetation C, soil organic C,
575 and evapotranspiration (Figure 7). CLASSIC reproduces observation-based estimates of global N
576 inputs, i.e., BNF, (as described in Section 4.1) as well as observation-based estimates of global N
577 losses (Table S4, Figure S6). Furthermore, CLASSIC estimates agree with other CMIP6 land
578 models (Table S4).

579 The global net atmosphere-land CO_2 flux or net biome productivity (NBP) is the critical
580 determinant of the performance of a land model because it ultimately affects atmospheric CO_2
581 concentration. Estimates of NBP from CLASSIC, CLASSIC-statN, and CLASSIC-C all lie
582 within the uncertainty range of estimates from the Global Carbon Project (Friedlingstein et al.,
583 2019) and thus all three versions of CLASSIC successfully reproduce the terrestrial C sink over
584 the late 20th century and early 21st century (Figure 8a). NBP estimates for the present day (1998
585 to 2018) when all global change drivers are acting concurrently are similar for all three versions
586 of CLASSIC. The difference between these three versions of CLASSIC is in how each responds
587 to individual global change drivers and, in particular, to atmospheric CO_2 concentration (Figure
588 8c). Present-day NBP for CLASSIC-C when atmospheric CO_2 concentration is acting in
589 isolation is the highest (3.9 Pg C yr^{-1}). Including N cycling reduces NBP: present-day NBP for
590 CLASSIC (1.4 Pg C yr^{-1}) is 44% lower than CLASSIC-C (i.e., a decrease of 2.5 Pg C yr^{-1}).
591 Furthermore, when BNF is not regulated by N limitation, NBP is even lower: present-day NBP
592 for CLASSIC-statN (0.9 Pg C yr^{-1}) is 64% lower than CLASSIC-C (i.e., a decrease of 3.0 Pg C
593 yr^{-1}). When all global change drivers are acting concurrently, the difference in present-day NBP
594 between CLASSIC and CLASSIC-statN is 0.2 Pg C yr^{-1} (1.3 Pg C yr^{-1} vs. 1.1 Pg C yr^{-1}) and is
595 the direct result of upregulated BNF driven by stronger N limitation under elevated atmospheric
596 CO_2 concentration which alleviates N limitation to some extent.

597 Historical NBP estimates of CLASSIC-C, which is the original version of CLASSIC, lie
598 within the uncertainty range of estimates from the Global Carbon Project (Friedlingstein et al.,
599 2019) because the strength of its CO_2 fertilisation effect has been adjusted to do so. Present-day
600 NBP when atmospheric CO_2 concentration is acting in isolation is higher for CLASSIC-C than
601 for CLASSIC and CLASSIC-statN (Figure 8c). This is because CLASSIC-C has been adjusted
602 to compensate for the effects of N deposition and elevated N mineralisation (due to elevated
603 temperature) over the historical period on NBP. Both these processes should stimulate NPP by
604 alleviating N limitation to some extent but they are not explicitly represented in CLASSIC-C.
605 While the absence of interactions between C and N cycling can be “accounted for” in historical
606 simulations by adjusting the strength of the CO_2 fertilisation effect, it has critical consequences
607 for future simulations which will encompass interacting and amplifying global change drivers.
608 This emphasises the importance of explicitly representing N cycling and the dynamic response of
609 vegetation to N limitation in land models.

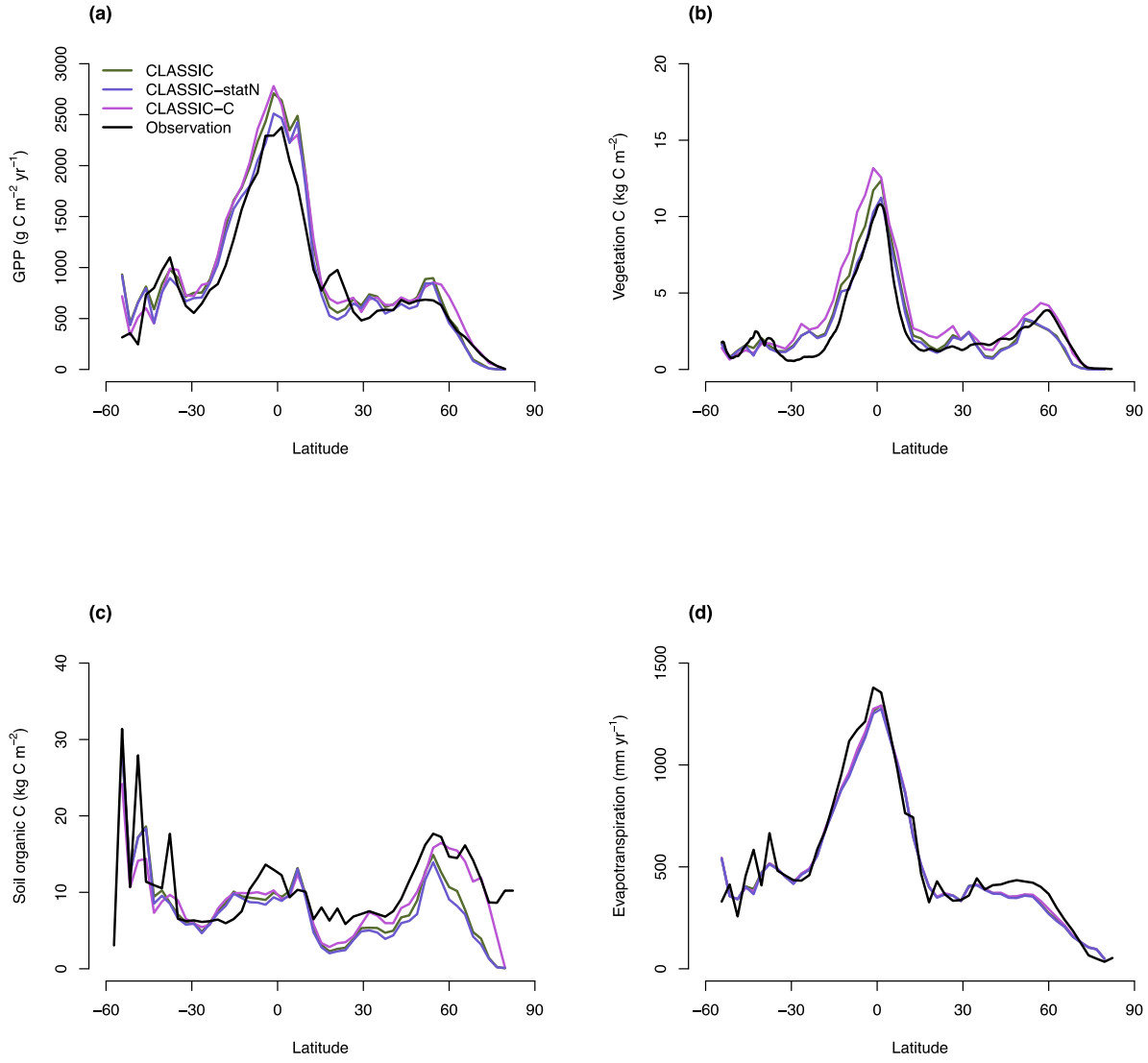

610

611 **Figure 7.** Latitudinal distributions of (a) gross primary productivity, (b) vegetation carbon, (c)
612 soil organic carbon, and (d) evapotranspiration (averaged over 1998 to 2018) simulated by
613 CLASSIC, CLASSIC without the regulation of BNF by N limitation (CLASSIC-statN), and
614 CLASSIC without N cycling (CLASSIC-C). Observation-based estimates are from (Beer et al.,
615 2010) for gross primary productivity, (Xu et al., 2021) for vegetation carbon, (Köchy et al.,
616 2015) for soil organic carbon, and (Martens et al., 2017) for evapotranspiration. Time series are
617 shown in Figure S7.

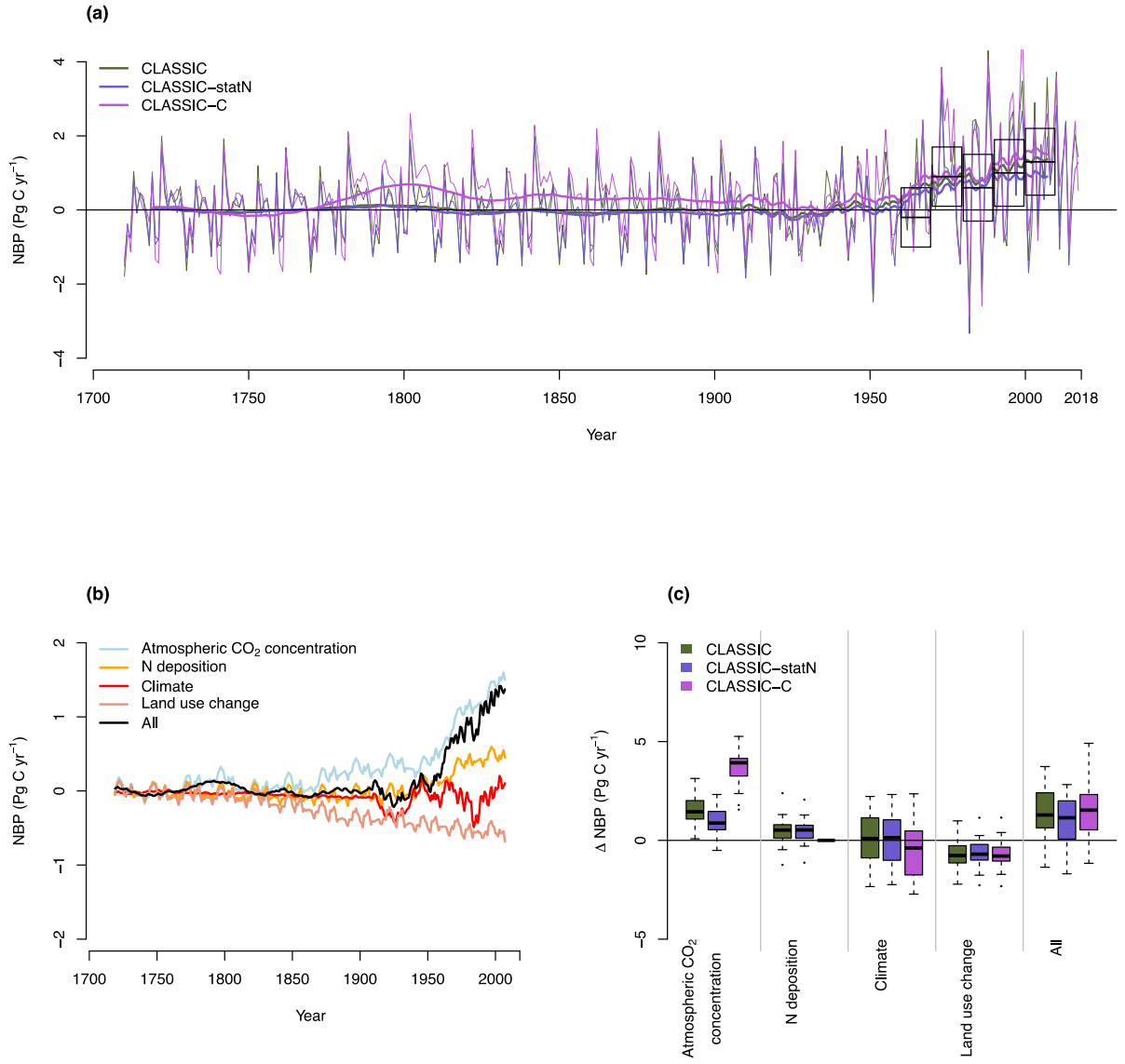

Figure 8. Net biome productivity over the historical period simulated by CLASSIC, CLASSIC without the regulation of BNF by N limitation (CLASSIC-statN), and CLASSIC without N cycling (CLASSIC-C). (a) Time series of net biome productivity simulated by CLASSIC, CLASSIC-statN, and CLASSIC-C over the historical period from 1701 to 2018 for all global change drivers concurrently. Boxes show the decadal mean and one standard deviation of observation-based estimates from the Global Carbon Project (Friedlingstein et al., 2019). (b) Time series of net biome productivity simulated by CLASSIC over the historical period from 1701 to 2018 for all global change drivers concurrently and individually. (c) Present-day (1998 to 2018) net biome productivity estimates simulated by CLASSIC, CLASSIC-statN, and CLASSIC-C (where the solid line indicates the median and the box extends from the first quartile to the third quartile).

5 Conclusions

Representing coupled C and N cycling in land models is a key challenge for projecting the terrestrial C sink. Although BNF is central to representing N cycling in land models given its key role in the dynamic response of vegetation to N limitation (Meyerholt et al., 2020; Peng et al., 2020; Wieder et al., 2015), it is challenging to evaluate simulated BNF against observation-based constraints due to the paucity of available data (Davies-Barnard & Friedlingstein, 2020). Simulating experimental manipulations of global change drivers and subsequently analysing the direction and magnitude of the response of BNF are an effective method for testing whether underlying mechanisms and thus the dynamic response of vegetation to N limitation via BNF are realistically represented. Our study shows that, without the regulation of BNF by N limitation, CLASSIC underestimates BNF increase under elevated CO_2 and simulates a BNF increase rather than a BNF decrease under N fertilisation. This leads to an underestimation of the NPP increase under elevated CO_2 and an overestimation of the NPP increase under N fertilisation, respectively. Without N cycling, CLASSIC overestimates NPP increase under elevated CO_2 and simulates no NPP change under N fertilisation.

Importantly, our study suggests that explicitly representing N cycling and the dynamic response of vegetation to N limitation of plant growth in land models is pivotal for realistically simulating the terrestrial C sink under global change. When the dynamic response of vegetation to N limitation via BNF is represented in CLASSIC, the present-day global net atmosphere-land CO_2 flux is decreased by 0.2 Pg C yr^{-1} in comparison to CLASSIC without N cycling. However, when the regulation of BNF by N limitation is not represented, the present-day global net atmosphere-land CO_2 flux is decreased by 0.4 Pg C yr^{-1} in comparison to CLASSIC without N cycling. The upregulation of BNF driven by stronger N limitation under elevated atmospheric CO_2 concentration thus alleviates N limitation. As such, representing the dynamic response of vegetation to N limitation via BNF increases the present-day terrestrial C sink by 0.2 Pg C yr^{-1}. Furthermore, while CLASSIC reproduces observations of the terrestrial C sink over the late 20th century and early 21st century regardless of whether N cycling is represented, CLASSIC without N cycling is only successful at doing so because the strength of the CO_2 fertilisation effect has been adjusted and thus compensates for the stimulatory influences of elevated N deposition and elevated N mineralisation (due to elevated temperature) on terrestrial C sequestration which are not represented. This has critical implications for projecting the future terrestrial C sink under interacting and amplifying global change drivers. Indeed, a former version of CLASSIC without N cycling (the coupled CLASS-CTEM framework) implemented within the 5th generation Canadian Earth System Model (CanESM5) yields one of the highest global net atmosphere-land CO_2 flux among CMIP6 Earth System Models under a high atmospheric CO_2 concentration scenario for the 21st century (Arora et al., 2020; Koven et al., 2021; Liddicoat et al., 2021). Thus, a mechanistic representation of N cycling and the dynamic response of vegetation to N limitation of plant growth in land models enables a more realistic representation of the response of the terrestrial C sink to global change drivers, providing confidence in projections of the future terrestrial C sink.

Acknowledgments

The authors would like to thank the input from the CLASSIC team (Paul Bartlett, Mike Brady, Salvatore Curasi, Joe Melton, Gesa Meyer, Christian Seiler, and Libo Wang).

The authors declare no conflicts of interest.

Open Research

The CLASSIC software container and all code for CLASSIC v.1.0 are available on the CLASSIC community Zenodo page (https://zenodo.org/communities/classic/?page=1&size=20).

References

Arora, V. K., & Boer, G. J. (2005a). A parameterization of leaf phenology for the terrestrial ecosystem component of climate models. *Global Change Biology*, *11*(1), 39–59. https://doi.org/10.1111/j.1365-2486.2004.00890.x

Arora, V. K., & Boer, G. J. (2005b). Fire as an interactive component of dynamic vegetation models. *Journal of Geophysical Research: Biogeosciences*, *110*(G2). https://doi.org/10.1029/2005jg000042

Arora, V. K., & Boer, G. J. (2010). Uncertainties in the 20th century carbon budget associated with land use change. *Global Change Biology*, *16*(12), 3327–3348. https://doi.org/10.1111/j.1365-2486.2010.02202.x

Arora, V. K., & Melton, J. R. (2018). Reduction in global area burned and wildfire emissions since 1930s enhances carbon uptake by land. *Nature Communications*, *9*(1), 1–10. https://doi.org/10.1038/s41467-018-03838-0

Arora, V. K., Boer, G. J., Christian, J. R., Curry, C. L., Denman, K. L., Zahariev, K., et al. (2009). The effect of terrestrial photosynthesis down regulation on the twentieth-century carbon budget simulated with the CCCma Earth System Model. *Journal of Climate*, *22*(22), 6066–6088. https://doi.org/10.1175/2009JCLI3037.1

Arora, V. K., Katavouta, A., Williams, R. G., Jones, C. D., Brovkin, V., Friedlingstein, P., et al. (2020). Carbon–concentration and carbon–climate feedbacks in CMIP6 models and their comparison to CMIP5 models. *Biogeosciences*, *17*(16), 4173–4222. https://doi.org/10.5194/bg-17-4173-2020

Asaadi, A., & Arora, V. K. (2021). Implementation of nitrogen cycle in the CLASSIC land model. *Biogeosciences*, *18*(2), 669–706. https://doi.org/10.5194/bg-18-669-2021

Asaadi, A., Arora, V. K., Melton, J. R., & Bartlett, P. (2018). An improved parameterization of leaf area index (LAI) seasonality in the Canadian Land Surface Scheme (CLASS) and Canadian Terrestrial Ecosystem Model (CTEM) modelling framework. *Biogeosciences*, *15*(22), 6885–6907. https://doi.org/10.5194/bg-15-6885-2018

Baig, S., Medlyn, B. E., Mercado, L. M., & Zaehle, S. (2015). Does the growth response of woody plants to elevated CO2 increase with temperature? A model-oriented meta-analysis. *Global Change Biology*, *21*(12), 4303–4319. https://doi.org/10.1111/gcb.12962

Beer, C., Reichstein, M., Tomelleri, E., Ciais, P., Jung, M., Carvalhais, N., et al. (2010). Terrestrial gross carbon dioxide uptake: Global distribution and covariation with climate. *Science*, *329*(5993), 834–838. https://doi.org/10.1126/science.1184984

710 Brookshire, E. N. J., Gerber, S., Menge, D. N. L., & Hedin, L. O. (2012). Large losses of
711 inorganic nitrogen from tropical rainforests suggest a lack of nitrogen limitation. *Ecology*
712 *Letters*, *15*(1), 9–16. https://doi.org/10.1111/j.1461-0248.2011.01701.x

713 Bytnerowicz, T. A., Akana, P., Griffin, K., & Menge, D. N. L. (2022). The temperature
714 sensitivity of woody dinitorgen fixation across species and growing temperatures. *Nature*
715 *Plants*. https://doi.org/10.1038/s41477-021-01090-x

716 Cheng, W., Parton, W. J., Gonzalez-Meler, M. A., Phillips, R., Asao, S., Mcnickle, G. G., et al.
717 (2014). Synthesis and modeling perspectives of rhizosphere priming. *New Phytologist*,
718 *201*(1), 31–44. https://doi.org/10.1111/nph.12440

719 Collatz, G. J., Ball, J. T., Grivet, C., & Berry, J. A. (1991). Physiological and environmental
720 regulation of stomatal conductance, photosynthesis and transpiration: a model that includes
721 a laminar boundary layer. *Agricultural and Forest Meteorology*, *54*(2), 107–136.
722 https://doi.org/10.1016/0168-1923(91)90002-8

723 Collatz, G. J., Ribas-Carbo, M., & Berry, J. (1992). Coupled Photosynthesis-Stomatal
724 Conductance Model for Leaves of C4 Plants. *Functional Plant Biology*, *19*(5), 519–538.
725 https://doi.org/10.1071/pp9920519

726 Davies-Barnard, T., & Friedlingstein, P. (2020). The Global Distribution of Biological Nitrogen
727 Fixation in Terrestrial Natural Ecosystems. *Global Biogeochemical Cycles*, *34*(3), 1–17.
728 https://doi.org/10.1029/2019GB006387

729 Davies-Barnard, T., Meyerholt, J., Zaehle, S., Friedlingstein, P., Brovkin, V., Fan, Y., et al.
730 (2020). Nitrogen cycling in CMIP6 land surface models: Progress and limitations.
731 *Biogeosciences*, *17*(20), 5129–5148. https://doi.org/10.5194/bg-17-5129-2020

732 Du, E., Terrer, C., Pellegrini, A. F. A., Ahlstrom, A., van Lissa, C. J., Zhao, X., et al. (2020).
733 Global patterns of terrestrial nitrogen and phosphorus limitation. *Nature Geoscience*, *13*(3),
734 221–226. https://doi.org/10.1038/s41561-019-0530-4

735 Elbert, W., Weber, B., Burrows, S., Steinkamp, J., Büdel, B., Andreae, M. O., & Pöschl, U.
736 (2012). Contribution of cryptogamic covers to the global cycles of carbon and nitrogen.
737 *Nature Geoscience*, *5*(7), 459–462. https://doi.org/10.1038/ngeo1486

738 Elser, J. J., Bracken, M. E. S., Cleland, E. E., Gruner, D. S., Harpole, W. S., Hillebrand, H., et al.
739 (2007). Global analysis of nitrogen and phosphorus limitation of primary producers in
740 freshwater, marine and terrestrial ecosystems. *Ecology Letters*, *10*(12), 1135–1142.
741 https://doi.org/10.1111/j.1461-0248.2007.01113.x

742 Elser, J. J., Fagan, W. F., Kerkhoff, A. J., Swenson, N. G., & Enquist, B. J. (2010). Biological
743 stoichiometry of plant production: Metabolism, scaling and ecological response to global
744 change. *New Phytologist*, *186*(3), 593–608. https://doi.org/10.1111/j.1469-
745 8137.2010.03214.x

746 Eyring, V., Bony, S., Meehl, G. A., Senior, C. A., Stevens, B., Stouffer, R. J., & Taylor, K. E.

(2016). Overview of the Coupled Model Intercomparison Project Phase 6 (CMIP6) experimental design and organization. *Geoscientific Model Development*, *9*(5), 1937–1958. https://doi.org/10.5194/gmd-9-1937-2016

Farquhar, G. D., von Caemmerer, S., & Berry, J. A. (1980). A biochemical model of photosynthetic CO2 assimilation in leaves of C3 species. *Planta*, *149*(1), 78–90. https://doi.org/10.1007/BF00386231

Finzi, A. C., Abramoff, R. Z., Spiller, K. S., Brzostek, E. R., Darby, B. A., Kramer, M. A., & Phillips, R. P. (2015). Rhizosphere processes are quantitatively important components of terrestrial carbon and nutrient cycles. *Global Change Biology*, *21*(5), 2082–2094. https://doi.org/10.1111/gcb.12816

Fowler, D., Coyle, M., Skiba, U., Sutton, M. A., Cape, J. N., Reis, S., et al. (2013). The global nitrogen cycle in the twenty-first century. *Philosophical Transactions of the Royal Society B: Biological Sciences*, *368*(1621), 20130164. https://doi.org/10.1098/rstb.2013.0164

Friedlingstein, P., Jones, M. W., O'Sullivan, M., Andrew, R. M., Hauck, J., Peters, G. P., et al. (2019). Global Carbon Budget 2019. *Earth System Science Data*, *11*(4), 1783–1838. https://doi.org/10.5194/essd-11-1783-2019

Haverd, V., Smith, B., Nieradzik, L., Briggs, P. R., Woodgate, W., Trudinger, C. M., et al. (2018). A new version of the CABLE land surface model (Subversion revision r4601) incorporating land use and land cover change, woody vegetation demography, and a novel optimisation-based approach to plant coordination of photosynthesis. *Geoscientific Model Development*, *11*(7), 2995–3026. https://doi.org/10.5194/gmd-11-2995-2018

Hedin, L. O., Brookshire, E. N. J., Menge, D. N. L., & Barron, A. R. (2009). The Nitrogen Paradox in Tropical Forest Ecosystems. *Annual Review of Ecology, Evolution, and Systematics*, *40*(1), 613–635. https://doi.org/10.1146/annurev.ecolsys.37.091305.110246

Hengl, T., De Jesus, J. M., Heuvelink, G. B. M., Gonzalez, M. R., Kilibarda, M., Blagotić, A., et al. (2017). SoilGrids250m: Global gridded soil information based on machine learning. *PLoS ONE*, *12*(2), e0169748. https://doi.org/10.1371/journal.pone.0169748

Herridge, D. F., Peoples, M. B., & Boddey, R. M. (2008). Global inputs of biological nitrogen fixation in agricultural systems. *Plant and Soil*, *311*(1), 1–18. https://doi.org/10.1007/s11104-008-9668-3

Houlton, B. Z., Wang, Y. P., Vitousek, P. M., & Field, C. B. (2008). A unifying framework for dinitrogen fixation in the terrestrial biosphere. *Nature*, *454*(7202), 327–330. https://doi.org/10.1038/nature07028

Kattge, J., Knorr, W., Raddatz, T., & Wirth, C. (2009). Quantifying photosynthetic capacity and its relationship to leaf nitrogen content for global-scale terrestrial biosphere models. *Global Change Biology*, *15*(4), 976–991. https://doi.org/10.1111/j.1365-2486.2008.01744.x

Kerkhoff, A. J., Fagan, W. F., Elser, J. J., & Enquist, B. J. (2006). Phylogenetic and growth form

784 variation in the scaling of nitrogen and phosphorus in the seed plants. *The American*
785 *Naturalist*, *168*(4), E103–E122. https://doi.org/10.1086/507879

786 Köchy, M., Hiederer, R., & Freibauer, A. (2015). Global distribution of soil organic carbon –
787 Part 1: Masses and frequency distributions of SOC stocks for the tropics, permafrost
788 regions, wetlands, and the world. *Soil*, *1*(1), 351–365. https://doi.org/10.5194/soil-1-351-
789 2015

790 Kou-Giesbrecht, S., Malyshev, S., Martínez Cano, I., Pacala, S. W., Shevliakova, E.,
791 Bytnerowicz, T. A., & Menge, D. N. L. (2021). A novel representation of biological
792 nitrogen fixation and competitive dynamics between nitrogen-fixing and non-fixing plants
793 in a land model (GFDL LM4.1-BNF). *Biogeosciences*, *18*(13), 4143–4183.
794 https://doi.org/10.5194/bg-18-4143-2021

795 Koven, C., Arora, V., Cadule, P., Fisher, R., Jones, C., Lawrence, D., et al. (2021). 23rd Century
796 surprises: Long-term dynamics of the climate and carbon cycle under both high and net
797 negative emissions scenarios. *Earth System Dynamics Discussions*, (April), 1–32.
798 https://doi.org/10.5194/esd-2021-23

799 Lau, W. K. M., Wu, H. T., & Kim, K. M. (2013). A canonical response of precipitation
800 characteristics to global warming from CMIP5 models. *Geophysical Research Letters*,
801 *40*(12), 3163–3169. https://doi.org/10.1002/grl.50420

802 Lawrence, D. M., Fisher, R. A., Koven, C. D., Oleson, K. W., Swenson, S. C., Bonan, G., et al.
803 (2019). The Community Land Model Version 5: Description of New Features,
804 Benchmarking, and Impact of Forcing Uncertainty. *Journal of Advances in Modeling Earth*
805 *Systems*, *11*(12), 4245–4287. https://doi.org/10.1029/2018MS001583

806 LeBauer, D. S., & Treseder, K. K. (2008). Nitrogen Limitation of Net Primary Productivity in
807 Terrestrial Ecosystems is Globally Distributed. *Ecology*, *89*(2), 371–379.
808 https://doi.org/10.1016/j.agee.2013.04.020

809 Liang, J., Qi, X., Souza, L., & Luo, Y. (2016). Processes regulating progressive nitrogen
810 limitation under elevated carbon dioxide: A meta-analysis. *Biogeosciences*, *13*(9), 2689–
811 2699. https://doi.org/10.5194/bg-13-2689-2016

812 Liddicoat, S. K., Wiltshire, A. J., Jones, C. D., Arora, V. K., Brovkin, V., Cadule, P., et al.
813 (2021). Compatible fossil fuel CO_2 emissions in the CMIP6 earth system models' historical
814 and shared socioeconomic pathway experiments of the twenty-first century. *Journal of*
815 *Climate*, *34*(8), 2853–2875. https://doi.org/10.1175/JCLI-D-19-0991.1

816 Long, S. P. (1991). Modification of the response of photosynthetic productivity to rising
817 temperature by atmospheric CO2 concentrations: Has its importance been underestimated?
818 *Plant, Cell & Environment*, *14*(8), 729–739. https://doi.org/10.1111/j.1365-
819 3040.1991.tb01439.x

820 Luo, Y., Su, B., Currie, W. S., Dukes, J. S., Finzi, A., Hartwig, U., et al. (2004). Progressive
821 Nitrogen Limitation of Ecosystem Responses to Rising Atmospheric Carbon Dioxide.

BioScience, *54*(8), 731–739. https://doi.org/10.1641/0006-3568(2004)054[0731:PNLOER]2.0.CO;2

Martens, B., Miralles, D. G., Lievens, H., Van Der Schalie, R., De Jeu, R. A. M., Fernández-Prieto, D., et al. (2017). GLEAM v3: Satellite-based land evaporation and root-zone soil moisture. *Geoscientific Model Development*, *10*(5), 1903–1925. https://doi.org/10.5194/gmd-10-1903-2017

McGroddy, M. E., Daufresne, T., & Hedin, L. O. (2004). Scaling of C:N:P stoichiometry in forests worldwide: Implications of terrestrial redfield-type ratios. *Ecology*, *85*(9), 2390–2401. https://doi.org/10.1890/03-0351

Melton, J. R., Shrestha, R. K., & Arora, V. K. (2015). The influence of soils on heterotrophic respiration exerts a strong control on net ecosystem productivity in seasonally dry Amazonian forests. *Biogeosciences*, *12*(4), 1151–1168. https://doi.org/10.5194/bg-12-1151-2015

Melton, J. R., Arora, V. K., Wisernig-Cojoc, E., Seiler, C., Fortier, M., Chan, E., & Teckentrup, L. (2020). CLASSIC v1.0: The open-source community successor to the Canadian Land Surface Scheme (CLASS) and the Canadian Terrestrial Ecosystem Model (CTEM)-Part 1: Model framework and site-level performance. *Geoscientific Model Development*, *13*(6), 2825–2850. https://doi.org/10.5194/gmd-13-2825-2020

Menge, D. N. L., Wolf, A. A., & Funk, J. L. (2015). Diversity of nitrogen fixation strategies in Mediterranean legumes. *Nature Plants*, *1*(6), 1–5. https://doi.org/10.1038/nplants.2015.64

Meyerholt, J., & Zaehle, S. (2015). The role of stoichiometric flexibility in modelling forest ecosystem responses to nitrogen fertilization. *New Phytologist*, *208*(4), 1042–1055. https://doi.org/10.1111/nph.13547

Meyerholt, J., Sickel, K., & Zaehle, S. (2020). Ensemble projections elucidate effects of uncertainty in terrestrial nitrogen limitation on future carbon uptake. *Global Change Biology*, *26*(7), 3978–3996. https://doi.org/10.1111/gcb.15114

Minchin, F. R., & Witty, J. F. (2005). Respiratory/Carbon Costs of Symbiotic Nitrogen Fixation in Legumes. In *Plant Respiration* (pp. 195–205). Dordrecht: Springer. https://doi.org/10.1007/1-4020-3589-6_11

O'Hara, G. W. (1998). The role of nitrogen fixation in crop production. *Journal of Crop Production*, *1*(2), 115–138. https://doi.org/10.1201/9780203745281

Peng, J., Wang, Y. P., Houlton, B. Z., Dan, L., Pak, B., & Tang, X. (2020). Global Carbon Sequestration Is Highly Sensitive to Model-Based Formulations of Nitrogen Fixation. *Global Biogeochemical Cycles*, *34*(1), e2019GB006296. https://doi.org/10.1029/2019GB006296

Phillips, R. P., Brzostek, E., & Midgley, M. G. (2013). The mycorrhizal-associated nutrient economy: A new framework for predicting carbon-nutrient couplings in temperate forests.

New Phytologist, *199*(1), 41–51. https://doi.org/10.1111/nph.12221

Le Quéré, C., Andrew, R. M., Friedlingstein, P., Sitch, S., Pongratz, J., Manning, A. C., et al. (2018). Global Carbon Budget 2018. *Earth System Science Data*, *10*(4), 2141–2194. https://doi.org/10.5194/essd-2017-123

Reed, S. C., Cleveland, C. C., & Townsend, A. R. (2011). Functional Ecology of Free-Living Nitrogen Fixation: A Contemporary Perspective. *Annual Review of Ecology, Evolution, and Systematics*, *42*(1), 489–512. https://doi.org/10.1146/annurev-ecolsys-102710-145034

Seiler, C., Melton, J., Arora, V., & Wang, L. (2021). CLASSIC v1.0: the open-source community successor to the Canadian Land Surface Scheme (CLASS) and the Canadian Terrestrial Ecosystem Model (CTEM) – Part 2: Global Benchmarking. *Geoscientific Model Development*, *14*(5), 2371–2417. https://doi.org/10.5194/gmd-2020-294

Sistla, S. A., & Schimel, J. P. (2012). Stoichiometric flexibility as a regulator of carbon and nutrient cycling in terrestrial ecosystems under change. *New Phytologist*, *196*(1), 68–78. https://doi.org/10.1111/j.1469-8137.2012.04234.x

Song, J., Wan, S., Piao, S., Knapp, A. K., Classen, A. T., Vicca, S., et al. (2019). A meta-analysis of 1,119 manipulative experiments on terrestrial carbon-cycling responses to global change. *Nature Ecology and Evolution*, *3*(9), 1309–1320. https://doi.org/10.1038/s41559-019-0958-3

Stocker, B. D., Prentice, I. C., Cornell, S. E., Davies-Barnard, T., Finzi, A. C., Franklin, O., et al. (2016). Terrestrial nitrogen cycling in Earth system models revisited. *New Phytologist*, *210*(4), 1165–1168. https://doi.org/10.1111/nph.13997

Sullivan, B. W., Alvarez-Clare, S., Castle, S. C., Porder, S., Reed, S. C., Schreeg, L., et al. (2014). Assessing nutrient limitation in complex forested ecosystems: Alternatives to large-scale fertilization experiments. *Ecology*, *95*(3), 668–681. https://doi.org/10.1890/13-0825.1

Sulman, B. N., Shevliakova, E., Brzostek, E. R., Kivlin, S. N., Malyshev, S., Menge, D. N. L., & Zhang, X. (2019). Diverse mycorrhizal associations enhance terrestrial C storage in a global model. *Global Biogeochemical Cycles*, *33*(4), 501–523. https://doi.org/10.1029/2018GB005973

Swart, N. C., Cole, J. N. S., Kharin, V. V, Lazare, M., Scinocca, J. F., Gillett, N. P., et al. (2019). The Canadian Earth System Model version 5 (CanESM5.0.3). *Geoscientific Model Development*, *12*(11), 4823–4873. https://doi.org/10.5194/gmd-12-4823-2019

Terrer, C., Vicca, S., Stocker, B. D., Hungate, B. A., Phillips, R. P., Reich, P. B., et al. (2018). Ecosystem responses to elevated CO_2 governed by plant-soil interactions and the cost of nitrogen acquisition. *New Phytologist*, *217*(2), 507–522. https://doi.org/10.1111/nph.14872

Terrer, C., Prentice, I., Jackson, R., Keenan, T., Kaiser, C., Vicca, S., et al. (2019). Nitrogen and phosphorus constrain the CO_2 fertilization of global plant biomass. *Nature Climate Change*, *9*(9), 684–689. https://doi.org/10.1038/s41558-019-0545-2

Thomas, R. Q., Brookshire, E. N. J., & Gerber, S. (2015). Nitrogen limitation on land: How can it occur in Earth system models? *Global Change Biology*, *21*(5), 1777–1793. https://doi.org/10.1111/gcb.12813

Verseghy, D. L. (1991). CLASS — A Canadian land surface scheme for GCMS. I. Soil model. *International Journal of Climatology*, *11*(2), 111–133.

Verseghy, D. L., McFarlane, N. A., & Lazare, M. (1993). CLASS — A Canadian land surface scheme for GCMS, II. Vegetation model and coupled runs. *International Journal of Climatology*, *13*(4), 347–370. https://doi.org/10.1002/joc.3370130402

Vitousek, P. M., Menge, D. N., Reed, S. C., & Cleveland, C. C. (2013). Biological nitrogen fixation: rates, patterns and ecological controls in terrestrial ecosystems. *Philosophical Transactions of the Royal Society B: Biological Sciences*, *368*(1621), 20130119. https://doi.org/10.1098/rstb.2013.0119

Walker, A. P., De Kauwe, M. G., Bastos, A., Belmecheri, S., Georgiou, K., Keeling, R. F., et al. (2020). Integrating the evidence for a terrestrial carbon sink caused by increasing atmospheric CO_2. *New Phytologist*, *229*(5), 2413–2445. https://doi.org/10.1111/nph.16866

Wang, Y. P., Law, R. M., & Pak, B. (2010). A global model of carbon, nitrogen and phosphorus cycles for the terrestrial biosphere. *Biogeosciences*, *7*(7), 2261–2282. https://doi.org/10.5194/bg-7-2261-2010

Weedon, J. T., Cornwell, W. K., Cornelissen, J. H. C., Zanne, A. E., Wirth, C., & Coomes, D. A. (2009). Global meta-analysis of wood decomposition rates: A role for trait variation among tree species? *Ecology Letters*, *12*(1), 45–56. https://doi.org/10.1111/j.1461-0248.2008.01259.x

Wieder, W. R., Cleveland, C. C., Lawrence, D. M., & Bonan, G. B. (2015). Effects of model structural uncertainty on carbon cycle projections: Biological nitrogen fixation as a case study. *Environmental Research Letters*, *10*(4), 044016. https://doi.org/10.1088/1748-9326/10/4/044016

Wright, S. J., Turner, B. L., Yavitt, J. B., Harms, K. E., Kaspari, M., Tanner, E. V. J., et al. (2018). Plant responses to fertilization experiments in lowland, species-rich, tropical forests. *Ecology*, *99*(5), 1129–1138. https://doi.org/10.1002/ecy.2193

Xu, L., Saatchi, S. S., Yang, Y., Yu, Y., Pongratz, J., Anthony Bloom, A., et al. (2021). Changes in global terrestrial live biomass over the 21st century. *Science Advances*, *7*(27), eabe9829. https://doi.org/10.1126/sciadv.abe9829

Yuan, Z. Y., Chen, H. Y. H., & Reich, P. B. (2011). Global-scale latitudinal patterns of plant fine-root nitrogen and phosphorus. *Nature Communications*, *2*(1), 1–6. https://doi.org/10.1038/ncomms1346

Zheng, M., Zhou, Z., Luo, Y., Zhao, P., & Mo, J. (2019). Global pattern and controls of biological nitrogen fixation under nutrient enrichment: A meta-analysis. *Global Change*

Biology, *25*(9), 3018–3030. https://doi.org/10.1111/gcb.14705

Zheng, M., Zhou, Z., Zhao, P., Luo, Y., Ye, Q., Zhang, K., et al. (2020). Effects of human disturbance activities and environmental change factors on terrestrial nitrogen fixation. *Global Change Biology*, *26*(11), 6203–6217. https://doi.org/10.1111/gcb.15328

Zhu, Q., Riley, W. J., Tang, J., Collier, N., Hoffman, F. M., Yang, X., & Bisht, G. (2019). Representing Nitrogen, Phosphorus, and Carbon Interactions in the E3SM Land Model: Development and Global Benchmarking. *Journal of Advances in Modeling Earth Systems*, *11*(7), 2238–2258. https://doi.org/10.1029/2018MS001571